RSL4 regulatory network acts as an early driver of root hair growth at low temperature in *Arabidopsis thaliana*

Tomás Urzúa Lehuedé[1,2,3,*], Victoria Berdion Gabarain[4,*], Tomas Moyano[1,3], Lucia Ferrero[5], Miguel Angel Ibeas[1,2,3], Hernan Salinas-Grenet[1,3], Gerardo Núñez-Lillo[6], Romina Acha[1,2], Jorge Perez[1,2], Florencia Perotti[5], Virginia Natali Miguel[5], Fiorella Paola Spies[5], Miguel A. Rosas[7], Michitaro Shibata[8], Diana R. Rodríguez-García[4], Adrian A. Moreno[1], Keiko Sugimoto[8], Karen Sanguinet[7], Claudio Meneses[2,9], Raquel L. Chan[5], Federico Ariel[5], Jose M. Alvarez[1,3], José M. Estevez[1,2,3,4,†]

[1]Centro de Biotecnología Vegetal, Facultad de Ciencias de la Vida, Universidad Andres Bello, Santiago, Chile.
[2]ANID - Millennium Science Initiative Program - Millennium Nucleus for the Development of Super Adaptable Plants (MN-SAP), Santiago, Chile.
[3]ANID - Millennium Science Initiative Program - Millennium Institute for Integrative Biology (iBio) Santiago, Chile.
[4]Fundación Instituto Leloir and IIBBA-CONICET. Av. Patricias Argentinas 435, Buenos Aires C1405BWE, Argentina.
[5]Instituto de Agrobiotecnología del Litoral, Universidad Nacional del Litoral-CONICET, Facultad de Bioquímica y Ciencias Biológicas, CCT Santa Fe, Colectora Ruta Nacional 168 km 0, Santa Fe 3000, Argentina.
[6]Escuela de Agronomía, Facultad de Ciencias Agronómicas y de los Alimentos, Pontificia Universidad Católica de Valparaíso, Calle San Francisco s/n, La Palma, Quillota 2260000, Chile.
[7]Department of Crop and Soil Sciences and Molecular Plant Sciences Graduate Program, Washington State University, Pullman, WA, 99164, USA.
[8]RIKEN Center for Sustainable Resource Science, Yokohama, 230-0045 and Department of Biological Sciences, Graduate School of Science, The University of Tokyo, 7-3-1 Hongo, Bunkyo-ku, Tokyo, 113-0033, Japan.
[9]Departamento de Fruticultura y Enología, Facultad de Agronomía e Ingeniería Forestal, Pontificia Universidad Católica de Chile, Santiago, Chile; Departamento de Genética Molecular y Microbiología, Facultad de Ciencias Biológicas, Pontificia Universidad Católica de Chile, Santiago, Chile; Fondo de Desarrollo de Áreas Prioritarias, Center for Genome Regulation, Santiago, Chile.

*Co-first authors.
†Correspondence should be addressed. Email: jose.estevez@unab.cl (J.M.E).

Abstract

The root hair (RH) cells can elongate to several hundred times their initial size, and are an ideal model system for investigating cell size control. Their development is influenced by both endogenous and external signals, which are combined to form a integrative response. Surprisingly, a low temperature condition of 10°C causes an increased RH growth in *Arabidopsis* and in several monocots, even when the development of the rest of the root and aerial parts of the plant are halted. Previously, we demonstrated a strong correlation between the growth response and a significant decrease in nutrient availability in the medium under low temperature conditions. However, the molecular basis responsible for receiving and transmitting signals related to the availability of nutrients in the soil, and their relation to plant development, remain largely unknown. We decided to further investigate the intricate molecular processes behind the particular responsiveness of this root cell type at low temperature. In this study, we have discovered a gene regulatory network (GRN) controlling early transcriptome responses to low temperature. This GNR is commanded by specific transcription factors (FTs), namely *ROOT HAIR DEFECTIVE 6-LIKE 4* (RSL4), a member of the homeodomain leucine zipper (HD-Zip I) group I 13 (AtHB13), the trihelix TF *GT2-LIKE1* (GTL1), and a previously unidentified MYB-like TF (AT2G01060). Furthermore, we have identified four downstream RSL4 targets *AtHB16*, *AtHB23*, *EARLY-RESPONSIVE TO DEHYDRATION 7* (ERD7) and ERD10 suggesting their participation in the regulation of RH development under these conditions. Functional analysis shows that such components of the RSL4-dependent transcriptional cascade influence the subsequent RH growth response to low temperature. These discoveries enhance our comprehension of how plants synchronize the RH growth in response to variations in temperature and nutrient availability at the cellular level.

Abstract Word counts 285

Text Word counts 5,944
Figures 1-5
Figure S1-S17
References 70

Introduction

Root hairs (RHs) are single cells that develop as a tubular protrusion from the root epidermis in a polar manner up to several hundred times their original size. RH differentiation is a complex process and consists of 3 stages: differentiation, initiation and elongation. The first is controlled by a developmental program involving transcription factor complexes (TFs) allowing or repressing the expression of the GL2 (GLABRA2) protein. This protein blocks RH development (Lin *et al.,* 2015) by inhibiting the transcription of the RHD6 (ROOT HAIR DEFECTIVE 6) regulator, which together with RSL1 can induce the expression of other factors such as RSL2 (Root Hair Defective 6 like 2) and RSL4 (ROOT HAIR DEFECTIVE 6 LIKE 4), thus allowing RH growth (Menand *et al.,* 2007; Yi *et al.,* 2010; Datta *et al.,* 2015; Proust *et al.,* 2016; Vijayakumar *et al.,* 2016; Lopez *et al.,* 2023). RHs are able to grow within hours in order to reach water-soluble nutrients in the soil, to promote interactions with the local microbiome, and to support the anchoring of the root. The overall fitness of plants is reduced in various loss-of-function RH mutants that lack RHs when grown in challenging soil conditions (Wu *et al.,* 2007, Haling *et al.,* 2013, Miguel *et al*., 2015). On the other hand, genotypes with longer RHs, achieved through the overexpression of ROOT HAIR DEFECTIVE 6-LIKE transcription factors (RSLs), have shown beneficial effects in species such as wheat (Han *et al.*, 2016, 2017), rice (Moon *et al*., 2019), and Brachypodium (Kim & Dolan, 2016). This highlights the deep importance of RHs in relation to plant development and physiology, despite not always receiving full recognition. It is known that intrinsic factors regulate RH elongation at the cellular level and external signals, among which we find morphogenetic programming, nutrient availability, and the action of different hormones (Casal & Estevez, 2021; Lopez *et al.,* 2023). Several works previously showed that RH growth is highly responsive to increasing nutrient concentrations in the media (Yi *et al.,* 2010; Bhosale *et al.,* 2018; Moison *et al.,* 2021; Jia *et al.,* 2023). While high nutrient concentrations impair RH development and growth, low concentrations of nutrients such as inorganic phosphate (Pi) and/or nitrates trigger a strong growth response mediated by the phytohormone auxin (Bhosale *et al.,* 2018; Mangano *et al.,* 2017; Jia *et al.,* 2023; Lopez *et al.,* 2023).

Recently it was shown that low temperature (10°C) is able to enhance RH growth possibly as a result of the restriction of nutrient mobility and accessibility by the root (Moison *et al.,* 2021; Martínez-Pacheco *et al.,* 2021). Conversely, an increase in agar concentration in the medium that restrains nutrient mobility resulted in the reversion of low temperature-induced RH elongation (Moison *et al.,* 2021). Altogether, these observations suggested that low temperatures restrict nutrient mobility and availability in the culture medium, leading to the promotion of polar RH growth. Despite these previous findings, the signals that trigger the RH cell elongation under these conditions are still unknown, but it is presumed that RHs could be highly susceptible to

116 environmental stresses such as temperature changes, triggering differences at the
117 transcriptomic and proteomic levels. Specifically, a novel ribonucleoprotein complex
118 composed by the lncRNA AUXIN-REGULATED PROMOTER LOOP (APOLO) and the TF
119 WRKY42 forms a regulatory hub to activate RHD6 by shaping its epigenetic environment
120 and integrating low temperature signals governing RH growth (Moison *et al.,* 2021;
121 Martínez-Pacheco *et al.,* 2021). Recently, new molecular components related to cell
122 wall-apoplastic related peroxidases, PRX62 and PRX69, were identified as important
123 factors for low temperature triggered RH growth by inducing changes in ROS
124 homeostasis and cell wall glycoprotein EXTENSIN insolubilization (Martinez-Pacheco *et*
125 *al.,* 2022). An autocrine regulation pathway between Rapid Alkalinization Factor 1
126 (RALF1) and the *Catharanthus roseus* RLK1-like (CrRLK1L) FERONIA (FER) receptor
127 phosphorylates the early translation factor eIF4E1 and produces RH-related proteins
128 including RSL4 to promote RH formation (Zhu *et al.,* 2020a,b). Finally, at low-
129 temperature, RHs showed a physical link between FER and TARGET OF RAPAMYCIN
130 COMPLEX (TORC). Mutants for *fer-4* and TORC components responded differently to
131 low nitrate than Col-0, and RHs remained stunted throughout the bulge stage
132 (Martinez-Pacheco *et al.,* 2023a). This FER-TORC pathway connects nutrients perception
133 at the cell surface with downstream responses in RH growth at low temperatures
134 (Martinez-Pacheco *et al.,* 2022). Although advances were achieved in our understanding
135 on how RH growth occurs at low temperature, the dynamic transcriptional cascade
136 controlling RH growth remains largely unknown, providing us with the opportunity to
137 find new key regulators in the process of RH elongation. Here, we provide a deep
138 characterization of how the TF RSL4 and main transcriptional network nodes AtHB13,
139 GTL1/DF1 and MYB-like as well as the downstream selected components
140 AtHB16/AtHB23 and ERD10/ERD7 are able to direct at early time points the gene
141 expression program that allows RH growth to respond to the low temperature. We
142 functionally validated these transcriptional nodes by gene expression assay, phenotypic
143 characterization of mutant/overexpressor and evaluation of genetic interactions. These
144 findings improve our understanding of how plants coordinate the development of their
145 RHs in response to changes in temperature and nutrient availability at the cellular level.
146
147
148 **Results**
149
150 **Low temperature effect on RH growth depends on nutrient availability.** Root hair (RH)
151 growth is a well conserved adaptive response to external low nutrients in the media-soil.
152 Previously, it was shown that at low temperature growth conditions (10°C), nutrients in
153 the media are reduced, which triggers a strong response in RH growth (Moison *et al.*,
154 2021; Martinez-Pacheco *et al*., 2021). Then, we assessed the effect of the low
155 temperature on RH growth, through a detailed temporal characterization of root
156 development (**Figure 1A**). Starting at 2 days of 10ºC, a significant effect on RH

157 elongation compared to control conditions was detected. This induction of growth
158 reached its peak at 3 days of low temperature treatment. Then, we decided to test if
159 small temperature changes around 10°C also trigger a similar RH growth effect. We
160 performed a temperature gradient from 22°C to 4°C in 2°C steps and maximum growth
161 was detected at 8-10°C (**Figure 1B**). From 8°C down to 4°C, the low temperature had a
162 negative effect on RH growth suggesting that the low temperature itself is more
163 deleterious than the linked low-nutrient effect. Based on this, we tested if a medium
164 with no nutrient content is able to repress the low temperature induced growth effect
165 on RHs. To this end, we used agarose that lacks any detectable nutrients and salts and
166 tested the low temperature growth effect (**Figure 1C**). In agreement with previous
167 evidence, when no nutrient is in the medium no low temperature effect is observed on
168 the RH growth, confirming that the signal is nutritional and not related to the
169 temperature itself as suggested before (Moison *et al.*, 2021; Martinez-Pacheco *et al.*,
170 2021; Martinez-Pacheco *et al*., 2023). Our data allowed us to use the low temperature
171 effect on RHs as a proxy of complex nutritional signals changes coming from the
172 medium. When we evaluated the effect of different pretreatment growth times, it was
173 observed that the final RH lengths in plants exposed to low temperatures were
174 equivalent whether plants were pre-grown for 7 or 14 days at 22°C, which was also the
175 case for their basal RH lengths (**Figure S1**). Since root light exposure generates a stress
176 that affects growth, hormonal signaling, abiotic responses, or nutrient starvation
177 adaptation compared with roots grown in the dark (Silva-Navas *et al.,* 2016), we
178 decided to test if direct light exposure might affect the RH growth intensity recorded
179 before. For this purpose, we used the system called D-Roots originally developed to
180 cultivate roots in darkness, including dark agar plugs and black-colored vertical plates
181 (Silva-Navas *et al.,* 2015). Using this D-root system, we have confirmed the previously
182 measured RH phenotypes at low temperature although with slightly higher magnitude
183 (**Figure 1C**). These results together showed that 8-10°C were the main temperature
184 trigger of RH growth affecting nutrient accessibility to the root surfaces and light
185 exposure does not significantly affect this growth process in RHs. Finally, we tested if
186 this enhancement on RH growth at low temperature is also present in monocots (**Figure**
187 **1D**) including *Brachypodium distachyon* (Bd21), rice (Kitaake), and wheat (Chinese
188 Spring). In these three cases we observed the same effect on RH growth at low
189 temperature as in Arabidopsis, although in these cases we tested them using 16 h:8 h
190 day:dark cycle (see methods). This last result highlighted that low temperature effect
191 on RH growth might be a broader response in plant roots, also applicable to these
192 monocots also.

193 **Genome wide transcriptional changes in roots exposed to low temperature.** RSL4 and
194 RSL2 have been identified as important regulators of RH growth in response both at
195 22°C and at low temperature, although RSL4 has been shown to be of higher relevance
196 than RSL2 in this role (Yi *et al.*, 2010; Moison *et al.,* 2021). Therefore, the loss of

197 function of RSL4, and RSL2 to a lower extent, would lead to changes in the transcript
198 abundance of direct and indirect RH gene targets. To identify all genes regulated by the
199 transcription factor (FT) RSL4 in the context of low temperature response, and to find
200 molecular factors involved in RH development that are dependent on RSL4, RSL2, or
201 both, we analyzed the transcriptome of *rsl2*, *rsl4*, and *rsl2 rsl4* genotypes in response to
202 low temperature treatments (2h and 6h) and compared it with the transcriptome of Wt
203 ecotype Columbia-0 (Col-0) plants (**Figure 2A**). Differential expression analysis was
204 performed and the number of genes was filtered considering an FC>|0.5| in at least
205 one condition. A total of 6,756 differentially expressed genes (DEG) were identified
206 between Col-0 and any of the mutant genotypes (**Figure S2** and **Figure S3**). The
207 heatmap in **Figure S2** shows the total number of DEGs identified, which were clustered
208 into 5 groups. Cluster 5 composed of 1,157 genes, which are positively regulated by
209 RSL2 and RSL4, is enriched with several GO terms related to RH development. To
210 identify genes whose expression depends on the interaction between low temperature
211 and the genotypes, we performed a two-way analysis of variance (ANOVA) analysis as
212 described previously (Alvarez *et al.,* 2014), considering temperature (T) and each
213 genotype (G). This analysis allows us to uncover genes for the interaction of TxG factors
214 whose response to temperature is affected in the mutants analyzed. Our analysis
215 identified 2,365 genes with a significant TxG factor for the *rsl4* mutant (**Figure 2B**).
216 These results were consistent with RSL4 being more influential in the RH response to
217 low temperature as compared to RSL2 (Moison *et al.*, 2021) in agreement with previous
218 evidence that show that RSL4 levels define the final RH length (Datta *et al.,* 2016). By
219 analyzing by heat map these 2,365 DEG, we identified three main clusters regulated by
220 RSL4 and also affected by low temperature (**Figure 2B**). GO analysis revealed several
221 processes related to RNA, virus replication and cold. In addition, the expression in
222 trichoblast and RH cells of RSL4 (and the related RHD6) were increased at early time
223 points of low temperature treatment while RSL2 was decreased (**Figure S4**). All this
224 evidence together indicates that the TF RSL4 is a major regulator of RH growth at low
225 temperature.

226 **RSL4 controls low temperature response through AtHB13-GTL1-MYB like transcription**
227 **factors.** To get insight into the regulatory cascade triggered by RSL4, we focused on the
228 2,365 genes that showed an altered response to low temperature in the *rsl4* mutant
229 (significant TxG factor). To investigate which TF might mediate the RSL4 effect of gene
230 expression in response to low temperature, we exploited the TF-target data allocated in
231 the ConnecTF database (Brooks *et al.,* 2021). The ConnecTF platform provides access to
232 a library of experimentally confirmed TF–target gene interaction datasets. To this end,
233 we used the list of differentially expressed TFs that depend on RSL4 and checked which
234 TF has available validated *in vitro* TF-binding data obtained by DNA Affinity Purification
235 sequencing (DAP-seq) (O'Malley *et al.*, 2016). We then reduced the list of possible
236 target genes to those genes highly or uniquely expressed in RH cells previously

237 identified by single cell RNA-seq or GFP-enriched protoplast studies (Brady *et al*., 2007;
238 Denyer *et al*., 2019; Jean-Baptiste *et al.*, 2019; Ryu *et al.*, 2019; Shulse *et al.*, 2019;
239 Zhang *et al.*, 2019) (**Figure 2C**). Then, we selected the top three TFs of the best five-
240 ranked list: (i) AtHB13, a class I HD-Zip TF previously described as involved in low
241 temperature response but not related to RH growth (Cabello *et al.,* 2012), (ii) a MYB-
242 like (AT2G01060) and (iii) GTL1, a previously characterized negative regulator of RH
243 growth under high nutrient condition, and its homologous DF1 (Shibata *et al.*, 2018,
244 2022). Based on this analysis, a RH gene regulatory network composed of 110 genes
245 controlled by RSL4 at low temperature was proposed (**Figure 2D**). Downstream of these
246 main regulators, we selected several members of the Arabidopsis HD-Zip I subfamily,
247 including AtHB16/AtHB23 and two TFs *EARLY-RESPONSIVE TO DEHYDRATION*
248 ERD7/ERD10 for further characterization. Notably, none of these TFs (unless RSL4) were
249 previously linked to RH growth at low temperature. This emphasizes the prognostic
250 capability of these integrated methodologies.

251 **The RSL4-dependent regulatory network regulates RH growth at low temperature**. To
252 validate the function of these RSL4-regulated gene regulatory networks in RH growth at
253 low temperature, we performed detailed RH phenotype screenings at 22°C and at 10°C
254 in loss of function mutants and overexpression lines for each component of the primary
255 and secondary regulatory network nodes as well as the upstream RSL4-regulator RHD6
256 (**Figures S5-S13** and **Figure 3A**). These include the TFs RSL4, AtHB13, GTL1/DF1 and
257 MYB-like as well as the downstream selected components AtHB16/AtHB23 and
258 ERD7/ERD10 (**Table S1**) (**Figure 3A-B**). Not surprisingly, several of the TFs analyzed
259 exhibited a changed RH growth at 10°C (**Figures S5-S13** and **Figure 3A**) providing strong
260 evidence of the predictive power of this combined bioinformatics-experimental
261 approach to identify key roles of specific TFs in certain environmental conditions.
262 According to our functional screening, the main nodes RSL4 (and RSL2) and the
263 downstream gene AtHB16 are positive regulators of RH growth at low temperature
264 while, on the other hand, GTL1-DF1 and AtHB3,13,20,23 emerged as negative RH
265 growth regulators at low temperature. A higher order of mutants for multiple HBs as
266 the quadruple mutant *athb3 (hat7) athb13 athb20 athb23* showed an enhanced RH
267 long phenotype at low temperature while single mutants *athb13* and *athb23* alone did
268 not, suggesting a high level of functional redundancy of these four HBs in RH growth at
269 low temperature. Surprisingly, *athb16* has a very short RH phenotype at low
270 temperature. This may indicate at least two contrasting roles for these HBs (AtHB16 vs
271 AtHB3,13,20,23) in RH growth at low temperature. To support the role of each TF on
272 the primary network on RH growth, we have quantified the expression levels of the
273 network's main nodes (*RSL4, AtHB13, GTL1/DF1* and *MYB-like*) at early temporal points
274 (0h (Basal, B), 2h, and 6h at 10°C) in selected mutant lines previously isolated and
275 characterized (**Figure S14-17**) (**Figure 3A-B**). In this manner, we are able to measure the
276 impact and influence of each of the main regulatory nodes identified in our network

277 over the expression of the selected gene from the proposed GRN. We found that RSL4-
278 GTL1 and GTL1-AtHB13 TFs form positive transcriptional feedback loops while RSL4-
279 AtHB13 forms a negative feedback loop (**Figure 3C-D**). This highlights a complex
280 transcriptional landscape behind a coherent phenotypic response, in this case at low
281 temperature even for single plant cells. To determine whether RSL4 controls the
282 expression of these main gene regulatory network nodes by direct binding to their
283 promoter regions, we searched for putative RSL4-binding sites (Hwang *et al.,* 2017) in
284 open chromatin regions, according to publicly available ATAC-seq datasets (Maher *et al.,*
285 2018). According to ChIP-qPCR using RSL4:RSL4-GFP plants and anti-GFP antibody, GTL1,
286 AtHB13 and MYB-like are direct RSL4 targets in the primary gene network and
287 AtHB16/AtHB23-ERD10 are their targets in the secondary network (**Figure 4A**), as
288 revealed in comparison to the previously identified direct target EXPANSIN 7 (EXP7)
289 (Hwang *et al.,* 2017). Overall, these results confirm that RSL4 positively controls the
290 expression of GTL1 and represses the expression of AtHB13 thus impacting RH growth.
291 It was also tested that presence of the GTL1 binding sites in the selected gene network
292 by ChIP-seq and positive peaks indicate direct regulation close to the starting
293 transcriptional sites for AtHB16 and ERD7/ERD10 only at room temperature suggestion
294 that the low temperature repressed its activity in these genes (**Figure 4B**). Finally, we
295 measured the expression levels on protein translational reporters for RSL4:RSL4-GFP
296 (and the related RHD6:RHD6-GFP), as well as the node GTL1:GTL1-GFP (and the related
297 DF1:DF1-GFP) (**Figure 4C-D** and **Figure S18**) both at room and at low temperature. All of
298 them except RSL4 were induced at low temperature in epidermal cells close to the RH
299 development and also in the differentiation zone. In addition, GUS staining of AtHB13,
300 AtHB16 and AtHB23 driven lines were also characterized (**Figure 4E**) and a strong signal
301 was detected for AtHB16, and to a lower extent, in AtHB23 in both low temperature
302 and room temperature. In sum, our systems biology approach identified new
303 components and relevant TF–target gene interactions that control RH growth in
304 responses to moderate cold. Our results indicate that RSL4 initiates an interconnected
305 transcriptional cascade by regulating GTL1, AtHB13, MYB-like and AtHB16/AtHB23 and
306 ERD10 as downstream gene targets. Consequently, GTL1 directly controls the
307 expression of RSL4 in a feedback loop and downstream moderate cold-responsive
308 genes (**Figure 5**). This last result in HBs mutants and reporters lines highlights the major
309 role of AtHB16 in controlling RH growth at low temperature. Overall, we were able to
310 experimentally confirm the function of these new regulatory components in low
311 temperature-controlled RH growth in Arabidopsis, establishing a complex regulatory
312 circuitry that integrates an environmental signal with RH development.

313

314 **Discussion**

315 In this work, we have extended the RH growth responses at low temperature to three
316 monocots in addition to *Arabidopsis thaliana* suggesting a more general growth
317 response than anticipated. We uncovered a regulatory map of RH growth under low
318 temperature in Arabidopsis by focusing on early time points (hours). We have
319 uncovered a new gene regulatory network controlled by RSL4 under low temperature
320 conditions that mediates RH growth using an RNA-seq filtered by DAP-seq and validated
321 expression profiling using mutant lines, coupled to ChIP approaches. Under the control
322 of RSL4 there are several TFs in the main network nodes such as AtHB13, GTL1/DF1 and
323 MYB-like as well as the downstream selected components AtHB16/AtHB23 and
324 ERD7/ERD10 (**Figure 5**). None of them were previously associated with low
325 temperature (unless HB13 and ERD7) and related to RH growth highlighting the
326 predictive power of this approach. Previously, based on single-cell RNA sequencing, it
327 was identified several TFs similar to our gene regulatory network (GRN) such as HB3
328 (HAT7) and GTL1 as responsive to brassinosteroids in the cortex during cell elongation
329 (Nolan et al. 2023). This suggests that similar GRN might be sub-functionalized in
330 different cellular contexts and under different environmental and hormonal cues. One
331 of the negative regulator of RH growth identified here is the trihelix TF GT2-LIKE1 (GTL1)
332 and its closest homolog, DF1, which stops RH cell growth by directly repressing RSL4 but
333 also bind to RHD6 preventing the activation of RSL4 (Shibata *et al.*, 2022) under excess
334 nutrient conditions (Shibata *et al*., 2018; Shibata *et al*. 2022) but it was not linked to low
335 temperature conditions. In our work, we found that GTL1 is positively controlled by
336 RSL4 and negatively regulates RH growth at low temperature with a similar function
337 described before linked to the nutrient availability and status present in the media.

338 Several members of the Arabidopsis HD-Zip I subfamily, AtHB13, AtHB16 and AtHB23,
339 were identified in this study as relevant TFs in the regulation of RH growth at moderate
340 low temperature (**Figure 5**). They belong to clade V (Arce *et al.,* 2011). They have a
341 leucine zipper (Zip) downstream the homeodomain (HD), located in the middle of the
342 protein (Viola *et al.,* 2016). Arabidopsis HD-Zip I members were classified based on their
343 exon-intron structure (Henriksson *et al.,* 2005) and subsequently based on
344 uncharacterized conserved motifs outside the HD-Zip (Arce *et al.,* 2011). HD-Zip I
345 proteins are only found in plants and have been linked to environmental stresses
346 (Perotti *et al.,* 2017) but also to many developmental processes (Ribone *et al.,* 2015;
347 Capella *et al.,* 2015; Perotti *et al.,* 2021; Perotti et al. 2022). AtHB13 provides enhanced
348 tolerance to both biotic and abiotic stresses, plays a role in pollen hydration and seed
349 germination (Hanson *et al.,* 2002; Cabello *et al.*, 2012; Gao et al. 2014; Silva *et al.,* 2016)
350 while AtHB23 participates in the elongation of the hypocotyl and the expansion of
351 cotyledons (Choi *et al.,* 2014), with functions in lateral root development (Perotti *et al.,*
352 2019; Perotti *et al.,* 2020; Perotti et al. 2021), together with PHL1 promotes
353 carbohydrate transport from pedicel-silique nodes to seeds (Spies *et al*., 2022), and is a
354 developmental modulator of root growth in normal and salinity conditions, by

355 interacting with PHL1 and MYB68 (Spies et al., 2023). Here, we found that AtHB13 is
356 negatively regulated by RSL4-GTL1 and positively regulated by MYB-like at low
357 temperature and participates in RH growth. It is plausible that AtHB13 do not act alone
358 since in the RSL4-regulated RH network at low temperature were also identified several
359 more HD-Zip I proteins. It remains to be tested if the contrasting growth roles of
360 AtHB16 and AtHB3,13,20,23 in the RH response to low temperature are conducted as
361 protein complexes or as individual TFs.

362 In addition, in this work, we uncovered one uncharacterized MYB-like TF as part of the
363 GRN that controls RH growth at low temperature. The MYB family, one of the biggest TF
364 groups in seed plants, consists of 197 members and this group is characterized by the
365 presence of a DNA-binding domain called the MYB DNA-binding domain (Riechmann *et*
366 *al.,* 2000) with a minimum of four repetitions of around 52 amino acids, which assemble
367 into a helix-turn-helix shape. The MYB-CC family consists of 15 members, which are
368 distinguished by the presence of both the MYB domain and a coiled-coil (CC) domain
369 (Rubio *et al.,* 2001). Here we identified a MYB-like TF (AT2G01060), currently not well
370 characterized, that regulates RH growth at low temperature. Finally, downstream RSL4-
371 GTL1 regulators, we have identified ERD7 and ERD10 proteins that belong to a small
372 family of highly conserved proteins that contain a PAM2 motif that may interact with
373 poly(A)-binding protein (Aalto et al., 2012). ERD7 is strongly upregulated by both biotic
374 and abiotic stresses such as cold, salt, excess light and Pi starvation (Cheng et al., 2013;
375 Rasmussen et al., 2013) and, it was found to be associated with lipids droplets via its C-
376 terminal senescence domain (SD) (Doner et al. 2021). Specifically, it binds to negatively
377 charged phospholipids, such as phosphatidylinositol (PI) and phosphatidic acid (PA) that
378 could induce structural and mechanical changes in the membrane that affect
379 membrane fluidity (Barajas-Lopez et al. 2021). In particular and in agreement with our
380 study, ERD7 is associated with low temperature stress. Overall, although our low
381 temperature condition is moderate, ERD7 and, possibly ERD10, might play a protective
382 role in the membrane stability during the RH cell expansion process.

383 Through our investigation of gene-expression patterns, we were able to uncover
384 potential TFs that potentially control RH growth responses to low temperature. The
385 incorporation of RH specific genes coupled to an early temporal data has a significant
386 favorable effect on the accuracy of our network predictions. Furthermore, our findings
387 served to identify novel TFs participating in the low temperature response triggering RH
388 growth. This highlights the significance of using spatiotemporal regulatory networks
389 when investigating specific biological inquiries. Our study enabled us to ascertain that
390 genes sensitive to low temperature and their associated biological processes are
391 regulated in a coordinated manner in both spatial and temporal dimensions. Together
392 with RSL4, the TFs AtHB3,13,20,23, AtHB16 and GTL1/DF1, have significant functions in
393 controlling the low temperature response in RH growth and the downstream changes in
394 gene expression eventually result in the enhancement of RH growth. These discoveries

395 enhance our comprehension of how plants synchronize the RH growth in response to
396 variations in temperature and nutrient availability at the cellular level. Future
397 challenges are related to the definition of the fine tune mechanisms of all these TFs
398 acting in real time in the control of RH genes. As a long term goal, these new RH
399 regulators identified here could be used to generate crops with enhanced RH growth to
400 tailored nutrient uptake to specific soil and temperature conditions.

401

402 **Materials and methods**

403

404 **Plant Material and Growth Conditions.** All the *Arabidopsis thaliana* lines used were in
405 the Columbia-0 (Col-0) background. All the plant lines sussed in this study are detailed
406 (**Table S1**). Seeds were surface sterilized and stratified in darkness at 4°C for 3 days
407 before being germinated on ½ strength 0,5X MS-MES (Duchefa, Netherlands) on 0.8%
408 Plant Agar™ (Duchefa, Netherlands) on 120 x 120 mm square petri dishes (Deltalab,
409 Spain) in a plant growth chamber in continuous light (120 µmol s^{-1} m^{-2}). For the RH
410 phenotype characterization, seeds were surface sterilized and stratified in darkness for
411 3 days at 4°C. Then grown on ½ strength MS agar plates, in a plant growth chamber at
412 22 °C in continuous light (120 µmol s^{-1} m^{-2}) for 7-14 days depending on the experiment
413 at 22°C as a pretreatment and then at 10°C (moderate-low temperature treatment) for
414 12, 24, 36, 48, 60 and 72 hours. Measurements were made between 7-17 days. For
415 quantitative analysis of RH phenotype, 10 fully elongated RHs were measured (using
416 the ImageJ software) from each root (n=20) grown by three biological replicates on
417 vertical agar plates. After treatment only new RH was measured. Images were captured
418 with a Leica EZ4 HD Stereo microscope (Leica, Germany) equipped with the LAZ ez
419 software.Results were expressed as the mean ± SD using the GraphPad Prism 8.0.1 (USA)
420 statistical analysis software.

421

422 **RH phenotype in monocots**. Plant species and varieties used include *Brachypodium*
423 *distachyon* (Bd21), rice (Kitaake), and wheat (Chinese Spring). All seeds were imbibed in
424 water for 2 hours and then surface sterilized with 0.6% hypochlorite and 1% Triton X-
425 100 with gentle shaking for 8 minutes. Seeds were then rinsed five times with sterile
426 water and then placed uniformly across ½ Murashige and Skoog (MS; PhytoTechnology
427 laboratories, USA), pH 5.7, 3% Gelzan (PhytoTechnology laboratories, USA) plates and
428 stored at 4°C for 3 d in the dark. For Arabidopsis, seeds rinsed with 70% ethanol and
429 then surface sterilized with 0.6% hypochlorite and 0.05% Triton X-100 with gentle
430 shaking for 5 minutes. Seeds were then rinsed five times with sterile water and placed
431 uniformly across ½ Murashige and Skoog (MS; PhytoTechnology laboratories, USA), 1%
432 sucrose, pH 5.7, 3% Gelzan (PhytoTechnology laboratories, USA) plates and stored at
433 4°C for 3 days in the dark. Plants were grown in a Conviron Adaptis growth chamber
434 model CMP6010 with a 16 h : 8 h, day : night cycle at a light intensity of 100 µmol m^{-2} s^{-1}

435 at 22°C. 3 fully elongated root hairs from the maturation zone were measured per root
436 after 8 d at 22°C and after 5 d at 22°C + 3d at 10°C. Images were captured using a M205
437 FA Leica Stereo microscope. The root length data is represented as a box blot with the
438 solid color dot representing the mean. The root hair density data are the mean±SE
439 (n=10–15 roots). A t-test was used to determine significant differences between the
440 means.
441
442 **RNA-seq analysis.** For the RNA-seq analysis, seedlings were grown on ½ strength MS
443 agar plates, in a plant growth chamber at 22 °C in continuous light (120 µmol s^{-1} m^{-2})
444 for 14 days at 22°C as a pre-treatment and then at 10°C (moderate-low temperature
445 treatment) for 2 and 6 hours. We analyzed a dataset with 12 factor groups (tree time
446 points: B, 2h, 6h) and four genotypes (Col-0, *rsl2*, *rsl4* and *rsl2 rsl4*) each with three
447 biological replicates giving 36 samples in total. Total RNA was extracted from 20–30 mg
448 of frozen root tissue. Frozen root samples were ground in liquid nitrogen and total RNAs
449 were extracted using E.Z.N.A Total RNA Kit I (Omega Bio-tek, Georgia, USA). RNA
450 quantity and purity were evaluated with a Qubit®2.0 fluorometer (Invitrogen™,
451 Carlsbad, CA, USA) using a Qubit™ RNA BR assay kit. RNA integrity and concentration
452 were assessed by capillary electrophoresis using an automated CE Fragment Analyzer™
453 system (Agilent Technologies, Santa Clara, CA, USA) with the RNA kit DNF-471-0500
454 (15nt). Total RNA-seq libraries were prepared according to the TruSeq Stranded Total
455 RNA Kit (Illumina, San Diego, CA, USA) following the manufacturer's instructions. Finally,
456 the constructed libraries were sequenced using Macrogen sequencing services (Seoul,
457 Korea) in paired end mode on a HiSeq4000 sequencer. For total RNA differential
458 expression analysis, a quality check was performed with FASTQC software (Andrews,
459 2010). Then, the adapter sequences were removed, reads with a quality score less than
460 30 and length less than 60 nucleotides were eliminated using Flexbar (Dodt *et al.,* 2012).
461 Resulting filtered reads were aligned against *Arabidopsis thaliana* Araport 11 genome
462 with the STAR aligner software. A total of 36 RNA libraries were sequenced, obtaining
463 an average of 84,741,219 reads for each one, with a minimum and maximum value of
464 72,658,864 and 102,182,242 reads, respectively. After filtering them by quality and
465 removing adapters, an average of 98.6% of the reads remained and after aligning them
466 against the *Arabidopsis thaliana* reference genome, between 88.1% (69,820,848) and
467 96.5% (93,740,042) of total reads were correctly aligned. For each library, the feature
468 Counts software from the Rsubread package (Liao *et al.,* 2019) was applied to assign
469 expression values to each uniquely aligned fragment. Differential gene expression
470 analysis was performed using the Bioconductor R edgeR package (Robinson *et al.,* 2010).
471 Differentially expressed genes (DEGs) were selected with an FDR < 0.05 and a Log2 FC >
472 |0.5|. To search for genetic functions and pathways overrepresented in the DEG lists,
473 genetic enrichment analysis was performed using the Genetic Ontology (GO) database
474 with the R package ClusterProfiler v4.0.5 (Yu *et al.,* 2012), using the compareCluster
475 function. The parameters used for this analysis were: lists of differentially expressed

476 genes for each comparison in ENTREZID, enrichGO sub-function, the universe from the
477 total of differentially expressed genes that present annotation as genetic background,
478 Benjamini-Hochberg statistical test and a filter of FDR less than 0.05. Subsequently, the
479 semantics filter of GO terms was performed using the simplify function of the same
480 package using a p-value and q-value cutoff less than 0.05.
481
482 **RT-qPCR analyses.** Total root RNA was extracted from these samples using the E.Z.N.A.
483 Total RNA Kit (Omega Bio-tek, Georgia, USA) according to the product's protocol. One
484 microgram of total RNA was reverse transcribed using an oligo$(dT)_{20}$ primer (Macrogen,
485 South Korea) and M-MLV Reverse Transcriptase™ (Invitrogen, USA) according to the
486 manufacturer's instructions. cDNA was then diluted 3-fold before qPCR analysis. qPCR
487 was performed on an AriaMx™ Real-time PCR System (Agilent, USA) using 10 uL of
488 Brilliant III Ultra-Fast SYBR Green Master-Mix (Stratagene, USA), 1 µL of cDNA, and 0.25
489 µM of each primer to a total volume of 20 µL per reaction. The *TAFII15* (AT4g31720)
490 gene was used as reference for normalization of gene expression levels. Statistical
491 analysis was performed using either parametric or non-parametric T-tests, after
492 determining the normality of the populations via the Shapiro-Wilk test. Results were
493 plotted showing mean and standard deviation. Primer used is detailed in **Table S2**.

494 **Network construction.** Direct and indirect targets of RSL4 were identified using the
495 RSL4 cis-motif reported in Hwang *et al.,* 2017 and the ConnecTF database. ConnecTF
496 was used to connect RSL4 to its indirect targets via TF2s that are themselves regulated
497 by RSL4 according to our RNA-seq analysis. We queried the ConnecTF database for all
498 the DAP-seq *in vitro* binding datasets. We restricted the results returned using Target
499 Genes filter with the list of differentially expressed genes according to our ANOVA
500 results for *rsl4* mutants (GxT genes). For this query, the TF2s were restricted using the
501 Filter TFs option with the list of TFs regulated by RSL4. Finally, the resulting network
502 was exported in the Network tab, combined with the direct TF-target information based
503 on RSL4 cis-motif, uploaded, and visualized using Cytoscape.
504
505 **TF-target list enrichment.** Using the Target Enrichment tab in ConnecTF, all the TF2s
506 that are enriched for RSL4 indirect targets were analyzed and visualized. The
507 significance of the overlap between TF–targets captured by DAP-seq in the list of RSL4
508 regulated targets was calculated. The P-values are calculated using Fisher's exact test
509 adjusted with the Bonferroni correction. The background set of genes used for the
510 calculation, which is by default all protein-coding genes for the Arabidopsis instances of
511 ConnecTF, were manually set by using the Background genes option in the query page.
512
513 **Chromatin immunoprecipitation (ChIP) PCR assay.** Chromatin immunoprecipitation
514 (ChIP) assays were performed on RSL4:RSL4-GFP plants (Moison *et al.* 2021) mainly as
515 described in (Ariel *et al.,* 2020). Plants were grown for 10 d in plates containing MS 0.5×

516 medium (pH 5.7; 0.8% agar) placed vertically in a culture chamber at 22 °C and
517 continuous light (120 µmol s^{-1} m^{-2}). After 10 d, the plates were placed horizontally and
518 treated with β-estradiol 10 μM solution for 3 h. The expression of RSL4 was checked by
519 qPCR. Chromatin was crosslinked with formaldehyde 1% (v/v) for 10 min at room
520 temperature. Crosslinking was stopped by adding glycine (125 mM final concentration)
521 and incubating for 10 min at room temperature. Crosslinked chromatin was extracted
522 by cell resuspension, centrifugation, cell membrane lysis, and sucrose gradient as
523 previously described (Ariel *et al.,* 2020). Nuclei were resuspended in Nuclei Lysis Buffer
524 and chromatin was sonicated using a water bath Bioruptor Pico (Diagenode; 30 s on/30
525 s off pulses, at high intensity for 10 cycles). Chromatin samples were incubated for 12 h
526 at 4 °C with Protein G Dynabeads (Invitrogen) precoated with the antibodies anti-FLAG
527 (Abcam ab18230) or anti-IgG (Abcam ab6702) as a negative control.
528 Immunoprecipitated DNA was recovered using Phenol:Chloroform: Iso-amilic Acid
529 (25:24:1; Sigma) and analyzed by qPCR using the primers listed in **Table S2.** One
530 upstream region of the EXP7 gene was used as a positive control (Hwang *et al.,* 2017).
531 Untreated sonicated chromatin was processed in parallel and considered the input
532 sample. The GraphPad Prism 6 software was used to analyze the data and produce the
533 graphs.
534
535 **GTL1 ChIP-seq analysis.** Illumina sequencing reads derived from ChIP and Input DNA of
536 GTL1 were mapped to the TAIR10 reference genome employing Bowtie2 for alignment.
537 Subsequently, the elimination of duplicate reads was performed. For the identification
538 of GTL1 ChIP peaks in relation to its corresponding Input DNA control, the MACS2
539 software was utilized with a significance threshold set at a q-value of 0.05. Post peak-
540 calling, gene annotation of the identified peaks was conducted utilizing BEDtools, which
541 incorporated a 2 kb region upstream from the transcription start site (TSS) for
542 consideration. The preparation of the sequencing data for visualization involved
543 filtering, ordering, and scaling of bam files, followed by conversion to bigwig format.
544 This conversion leveraged the "bamCoverage" function within deepTools 2.0,
545 configured with a bin size of 10 bp, RPKM normalization, and a smooth length of 60.
546 Visual representations of the genomic data displayed in Figure 4B were generated using
547 the Integrative Genomics Viewer (IGV)(reference: 10.1093/bib/bbs017).
548
549 **Confocal Microscopy**. Confocal laser scanning microscopy for the lines RSL4:RSL4-GFP,
550 RSL2:RSL2-GFP, RHD6:RHD6-GFP, GTL1:GTL1-GFP and DF1:DF1-GFP was performed
551 using Zeiss LSM5 Pascal (Zeiss, Germany) (Excitation: 488 nm argon laser; Emission:
552 490–525 nm, Zeiss Plain Apochromat 10X/0.30 or 40X/1.2 WI objectives according to
553 experiment purpose). Z stacks were done with an optical slice of 1 µm, and fluorescence
554 intensity was measured at the RH tip. The scanning was performed using confocal laser
555 scanning microscopy Zeiss LSM 710 (Carl Zeiss, Germany). For image acquisition,
556 20x/1.0 NA Plan-Apochromat objective for root tips were used. The GFP signal was

557 excited with a 488 nm argon laser at 4% laser power intensity and emission band of
558 493-549 nm. Propidium Iodide signal was excited with a 488 nm argon laser at 4% laser
559 power intensity and emission band 519-583 nm. GFP signal at the RH tip were
560 quantified using the ImageJ software. Fluorescence AU was expressed as the mean ± SD
561 using the GraphPad Prism 8.0.1 (USA) statistical analysis software. Results are
562 representative of two independent experiments, each involving 10–15 roots.
563
564
565 **Acknowledgements**
566 We would like to thank xxxx for the seed lines. We thank NASC (Ohio State University)
567 for providing T-DNA lines seed lines, Trevor Nolan (Phillip Benfey group) for the
568 quadruple HB mutant, J.M.E., F.A. and R.L.C. are investigators of the National Research
569 Council (CONICET) from Argentina. M.I. is supported by ANID FONDECYT
570 POSTDOCTORADO [grant 3220138]. This work was supported by grants from ANPCyT
571 (PICT2019-0015 and PICT2021-0514), by ANID – Programa Iniciativa Científica Milenio
572 ICN17_022, NCN2021_010 and Fondo Nacional de Desarrollo Científico y Tecnológico
573 [1200010] to J.M.E. J.M.A lab is supported by ANID FONDECYT 1210389, Programa
574 Iniciativa Científica Milenio ICN17_022, and NSF Plant Genome Grant NSF-PGRP: IOS-
575 1840761.
576
577
578 **Author Contribution**
579 T.U.L. and V.B.G performed most of the experiments, analyzed the data and helped in
580 the writing process of the manuscript. M.A.I. and H.S-G. performed some experiments
581 and helped in the writing process. G.N-L. and C.M. performed the RNA-seq analysis, T.M.
582 and J.M.A. performed the gene network analysis and helped on the writing process. L.F.
583 and F.A. carried out the ChIP experiment of RSL4 and helped on the writing process.
584 R.M. and K.S. carried out the root hair characterization in monocots. A.A.M. helped in
585 the writing process. M.S. and K.S. provided seeds and helped in the writing process.
586 R.L.C. provide AtHBs lines and help in the writing process. J.M.E. designed research,
587 analyzed the data, supervised the project, and wrote the paper. All authors commented
588 on the results and the manuscript. This manuscript has not been published and is not
589 under consideration for publication elsewhere. All the authors have read the
590 manuscript and have approved this submission.
591
592 **Competing financial interest**
593 The authors declare no competing financial interests. Correspondence and requests for
594 materials should be addressed to J.M.E. (Email: jose.estevez@unab.cl). HD-Zip mutants
595 and overexpressor lines must be requested to R.L.C.

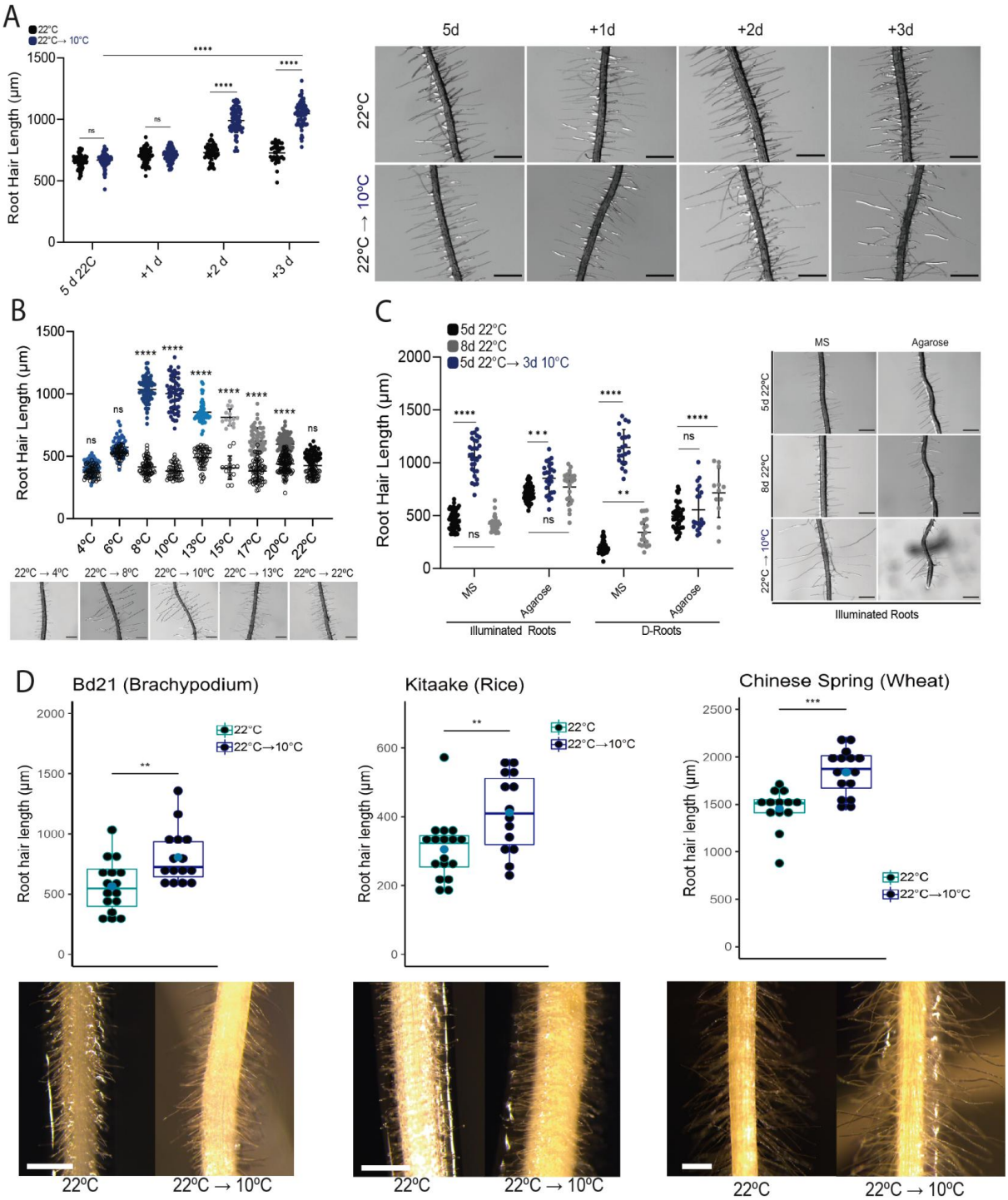

Figure 1. Low temperature effect on RH growth in Arabidopsis and monocots. (**A**) Low-temperature RH growth up to 3 days of treatment. (**B**) Temperature fluctuations impact on RH growth and growth maxima was detected at 8-10°C. (**C**) A nutrient-free medium can suppress the low-temperature growth impact on RHs. The previously recorded RH traits at low temperature were verified with somewhat larger magnitude using this D-root method. (A-C) Each point is the mean of the length of the 5 longest RHs identified in the maturation zone of a single root. Data are the mean ± SD (N= 30 roots), two-way ANOVA followed by a Tukey–Kramer test; (****) p <0.001, NS= non-significant. Results

605 are representative of three independent experiments. Asterisks indicate significant
606 differences between Col-0 and the corresponding treatment at the same temperature
607 or between the same treatment at different temperatures. Representative images of
608 each genotype are shown on the right. Scale bars= 500 µm. (**D**) Low-temperature
609 triggers an enhancement on RH growth in the monocots *Brachypodium distachyon*
610 (Bd21), rice (Kitaake), and wheat (Chinese Spring). Representative pictures are shown in
611 the bottom. Scale bars= 500 µm. Data are the mean ± SD (N= 30 roots), two-way
612 ANOVA followed by a Tukey–Kramer test; (**) $p < 0.01$, (***) $p < 0.001$, NS= non-
613 significant.

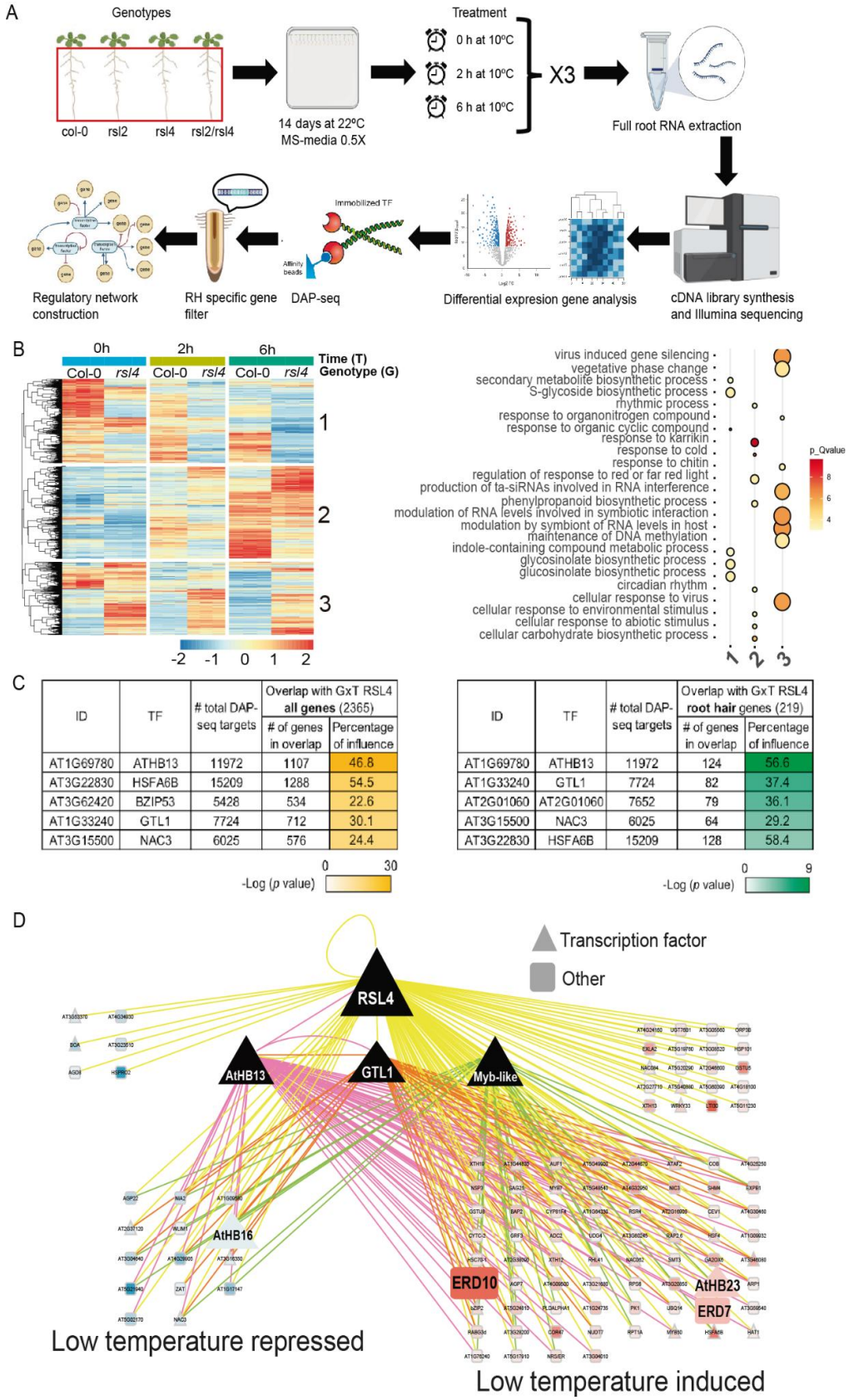

ID	TF	# total DAP-seq targets	Overlap with GxT RSL4 **all genes** (2365)	
			# of genes in overlap	Percentage of influence
AT1G69780	ATHB13	11972	1107	46.8
AT3G22830	HSFA6B	15209	1288	54.5
AT3G62420	BZIP53	5428	534	22.6
AT1G33240	GTL1	7724	712	30.1
AT3G15500	NAC3	6025	576	24.4

0 30
-Log (*p* value)

ID	TF	# total DAP-seq targets	Overlap with GxT RSL4 **root hair** genes (219)	
			# of genes in overlap	Percentage of influence
AT1G69780	ATHB13	11972	124	56.6
AT1G33240	GTL1	7724	82	37.4
AT2G01060	AT2G01060	7652	79	36.1
AT3G15500	NAC3	6025	64	29.2
AT3G22830	HSFA6B	15209	128	58.4

0 9
-Log (*p* value)

Figure 2. Identification of the RH specific RSL4-mediated gene regulatory network acting at low temperature on an early temporal window. (**A**) Dual bioinformatic-experimental strategies using RNA-seq plus DAP-seq prediction followed to identify the

619 RH specific RSL4-transcriptional network at early times at low temperature. (**B**)
620 Differential expression analysis by a heat map of the transcriptome of Wt Col-0 and *rsl4*
621 genotypes in response to low temperature treatments (2h and 6h). A two-way analysis
622 of variance (ANOVA) analysis was carried out, considering temperature (T) and each
623 genotype (G) as factors and controlling type I error using the false discovery rate. A total
624 of 2,365 DEG showed an altered response to low temperature in the *rsl4* mutant
625 (significant TxG factor) were grouped into 3 clusters. (**C**) Best 5-ranked list of TFs based
626 on the overall overlap of 2,365 genes controlled by RSL4 with DAP-seq common targets
627 (on the left) and RSL4-specifically expressed in RHs (on the right) using the ConnecTF
628 database. (**D**) Gene regulatory RSL4-network acting on RH growth at low temperature
629 after 6h of exposure. Genes are drawn as triangles (TF, transcription factors) and
630 squares (target genes). Lines indicate predicted transcriptional activation or predicted
631 transcriptional repression. Yellow lines indicate RSL4, red line AtHB13 and green lines
632 MYB-like putative TFs binding site by DAP-seq in the upstream region of the
633 corresponding genes.

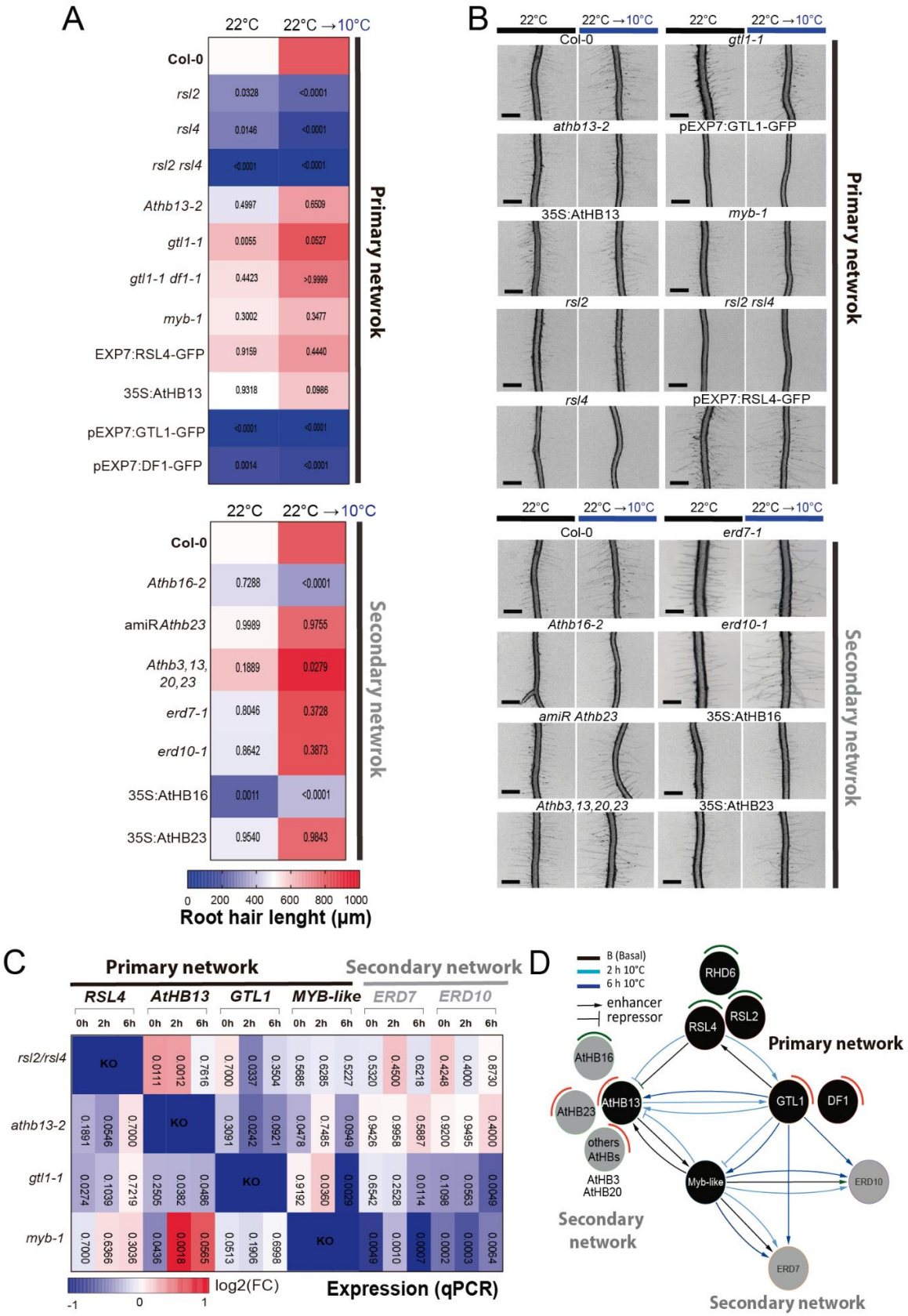

Figure 3. Major nodes of the RSL4-transcriptional primary and secondary network impact on RH phenotypes linked to gene expression changes at low temperature. (A)

637 Heatmap of the RH phenotype at 22°C and 10°C of the different mutants and
638 overexpression lines of the main network nodes RSL4 (and RSL2), AtHB13, GTL1/DF1
639 and MYB-like as well as the downstream selected components AtHB16/AtHB23 and
640 ERD7/ERD10. Blue color scale represents the length of RH in µm (0-1500). Pair
641 comparisons are made between Col-0 and each line (see **Table S1** and **Figures S5-S12**).
642 Data are the mean ± SD (N=20 roots), two-way ANOVA followed by a Tukey–Kramer test;
643 p-values are shown. (**B**) Representative images of RH phenotype of Col-0, GTL1, MYB-
644 like (At2G01060) and AtHB13 as well as RSL2-RSL4 quantified in (A). Scale bars = 1000
645 µm. (**C**) Heatmap of the gene expression analysis of the network main nodes TFs RSL4,
646 AtHB13 and GTL1/DF1 and as well as the downstream selected components
647 ERD7/ERD10 in each mutant/overexpression line previously isolated and characterized
648 (**Figures S12-S16**). Data are the mean of three biological replicates, two-way ANOVA
649 followed by a Tukey–Kramer test; p-values are shown. (**D**) Main transcriptional nodes of
650 the RSL4 network with the detailed effect of each component at transcriptional and RH
651 phenotypic levels. Arrows indicate positive gene expression regulation and blunt arrows
652 indicate transcriptional repression. Green curved line means positive RH growth
653 regulation and red curved line means negative RH growth regulation.

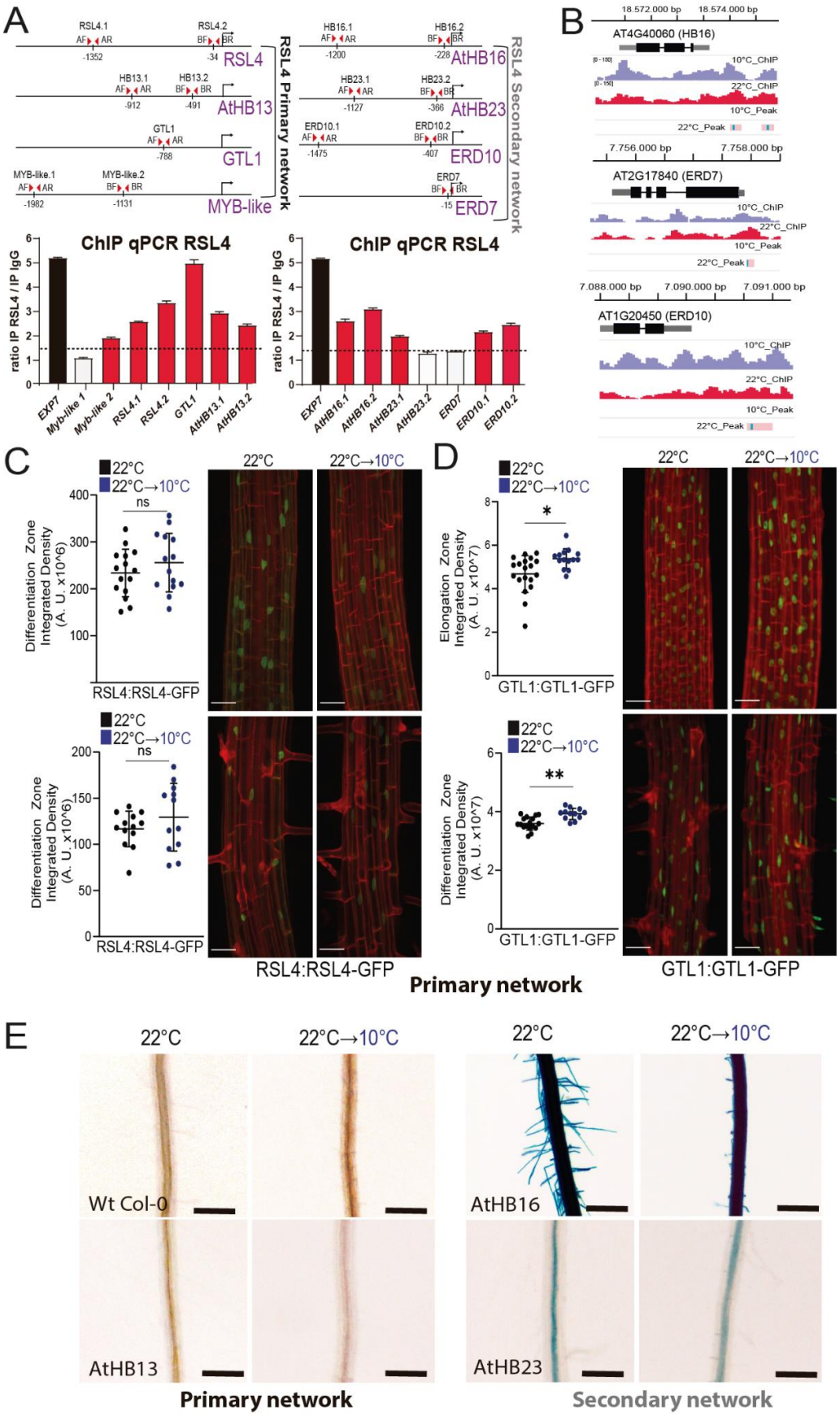
A
RSL4.1
RSL4.2
RSL4
HB13.1
HB13.2
AtHB13
GTL1
MYB-like.1
MYB-like.2
MYB-like
RSL4 Primary network
HB16.1
HB16.2
AtHB16
HB23.1
HB23.2
AtHB23
ERD10.1
ERD10.2
ERD10
ERD7
RSL4 Secondary network
ChIP qPCR RSL4
ratio IP RSL4 / IP IgG
EXP7
Myb-like 1
Myb-like 2
RSL4.1
RSL4.2
GTL1
AtHB13.1
AtHB13.2
AtHB16.1
AtHB16.2
AtHB23.1
AtHB23.2
ERD7
ERD10.1
ERD10.2
B
AT4G40060 (HB16)
AT2G17840 (ERD7)
AT1G20450 (ERD10)
10°C_ChIP
22°C_ChIP
10°C_Peak
22°C_Peak
C
22°C
22°C→10°C
ns
Differentiation Zone Integrated Density (A. U. x10^6)
RSL4:RSL4-GFP
D
*
**
Elongation Zone Integrated Density (A. U. x10^7)
Differentiation Zone Integrated Density (A. U. x10^7)
GTL1:GTL1-GFP
Primary network
E
Wt Col-0
AtHB16
AtHB13
AtHB23
Primary network
Secondary network

654

655 **Figure 4. Regulation of RSL4 on the main transcriptional nodes and selected**
656 **downstream target genes and low temperature effect on main TFs reporters**
657 **expression**.
658 (**A)** ChIP-qPCR analysis of RSL4 binding to primary and secondary RSL4 nodes gene
659 targets promoter regions at low temperature. Schemes of the loci showing the location
660 of the fragments analyzed by ChIP-qPCR are shown in the upper part (A = Primer A; B =
661 Primer B; F = Primer forward; R = Primer reverse). Primers were designed analyzing
662 ATAC-seq experiments in regions where the chromatin is accessible (Maher *et al.,* 2018).
663 *EXP7* oligos were used as positive controls (xxxx). The data are mean ± SD of 2 technical
664 replicates. The experiment was performed twice with similar results. The enrichment
665 was measured relative to the negative control ACTIN. **(B)** ChIP-seq analysis of GTL1
666 binding on HB16, ERD7/ERD10 as secondary RSL4 nodes gene targets promoter regions
667 only at room temperature. Schemes of the loci. (**C-D**). Effect of the low temperature on
668 the expression of GTL1 and RSL4 in the elongation and differentiation root zones. (**C**)
669 Confocal images of GTL1:GTL1-GFP in *gtl-1* translational reporter line of at 22°C and
670 after transfer from ambient to low temperature (22°C→10°C). Quantitative evaluation
671 of the GFP fluorescence intensity across the root elongation zones at 22°C and after
672 transfer from ambient to low temperature. Fluorescence intensity is expressed in
673 arbitrary units (A.U.), N=6-8 roots. Results are representative of three independent
674 experiments. Scale bars=50 µm. (**D**) Confocal images of RSL4:RSL4-GFP translational
675 reporter line of at 22°C and after transfer from ambient to low temperature
676 (22°C→10°C). Quantitative evaluation of the GFP fluorescence intensity across the root
677 elongation zones at 22°C and after transfer from ambient to low temperature.
678 Fluorescence intensity is expressed in arbitrary units (A.U.), N=6-8 roots. Results are
679 representative of three independent experiments. Scale bars=50 µm. (**D**) Confocal
680 images of RSL4:RSL4-GFP translational reporter line of at 22°C and after transfer from
681 ambient to low temperature (22°C→10°C). Quantitative evaluation of the GFP
682 fluorescence intensity across the root elongation zones at 22°C and after transfer from
683 ambient to low temperature. Fluorescence intensity is expressed in arbitrary units
684 (A.U.), N=8 roots. Results are representative of three independent experiments. Scale
685 bars=50 µm. (**E**) Expression in roots of GUS reporter lines for AtHB13, AtHB16 and
686 AtHB23 at 22°C and after transfer from ambient to low temperature (22°C→10°C).
687 Images are representative of three independent experiments. Scale bars=200 µm.

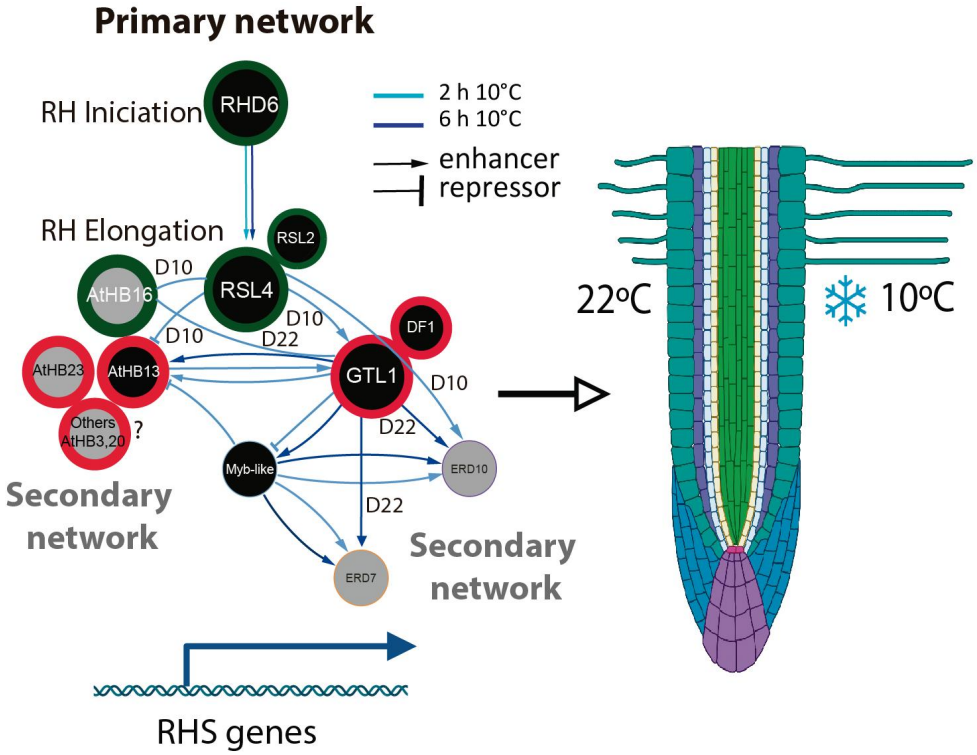

Figure 5. Proposed model of RSL4-regulation of RH growth at low temperature at early times (2-6 hs). Main transcriptional nodes of the RSL4-regulated network with the detailed effect of each component at transcriptional and RH phenotypic levels. Red circles indicate that repress RH growth at low temperature and Green circles are enhancers of RH growth. Direct regulation at 10°C/22°C (D10/D22) was assessed by ChIP results. Arrows indicate positive gene expression regulation and blunt arrows indicate transcriptional repression. (?) Indicates that needs to be experimentally validated. RHS= Root Hair Specific genes.

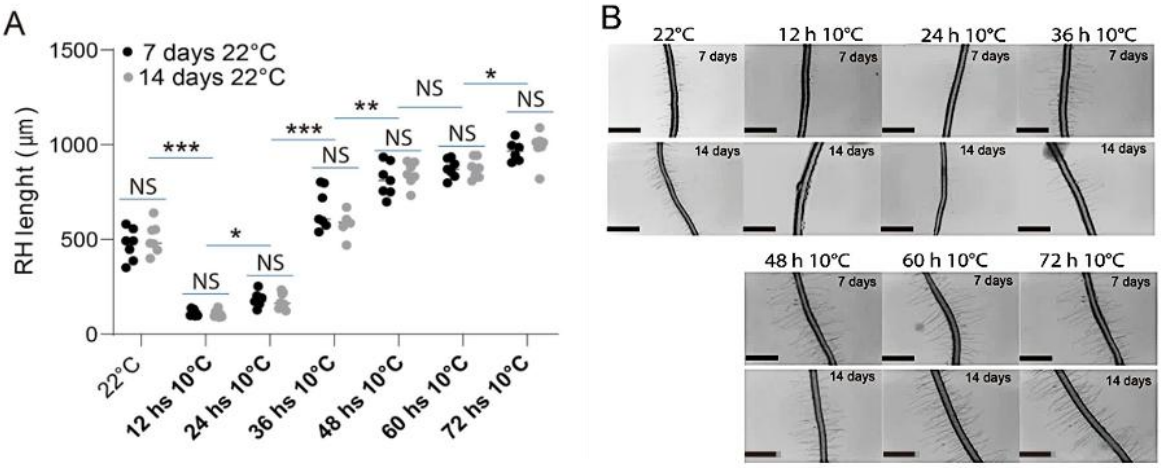

Figure S1. Influence of room temperature pretreatment time length on low temperature root hair growth in Arabidopsis thaliana. (**A**) quantification of RH length at different treatment times at 22°C prior to cold exposure (7 and 14 days) and different cold exposure times (0, 12, 24, 36, 48, 60 and 72 hours) in both pretreatment conditions. (**B**) visualization by stereo microscopy of the phenotypic data represented. Data are the mean ± SD (N=20 roots), two-way ANOVA followed by a Tukey–Kramer test; (*) $p < 0.05$, (**) $p < 0.01$, (***) $p < 0.001$, NS=non-significant. Results are representative of three independent experiments. Asterisks indicate significant differences between Col-0 and the corresponding genotype at the same temperature. Representative images of each genotype are shown below. Scale bars= 500 µm.

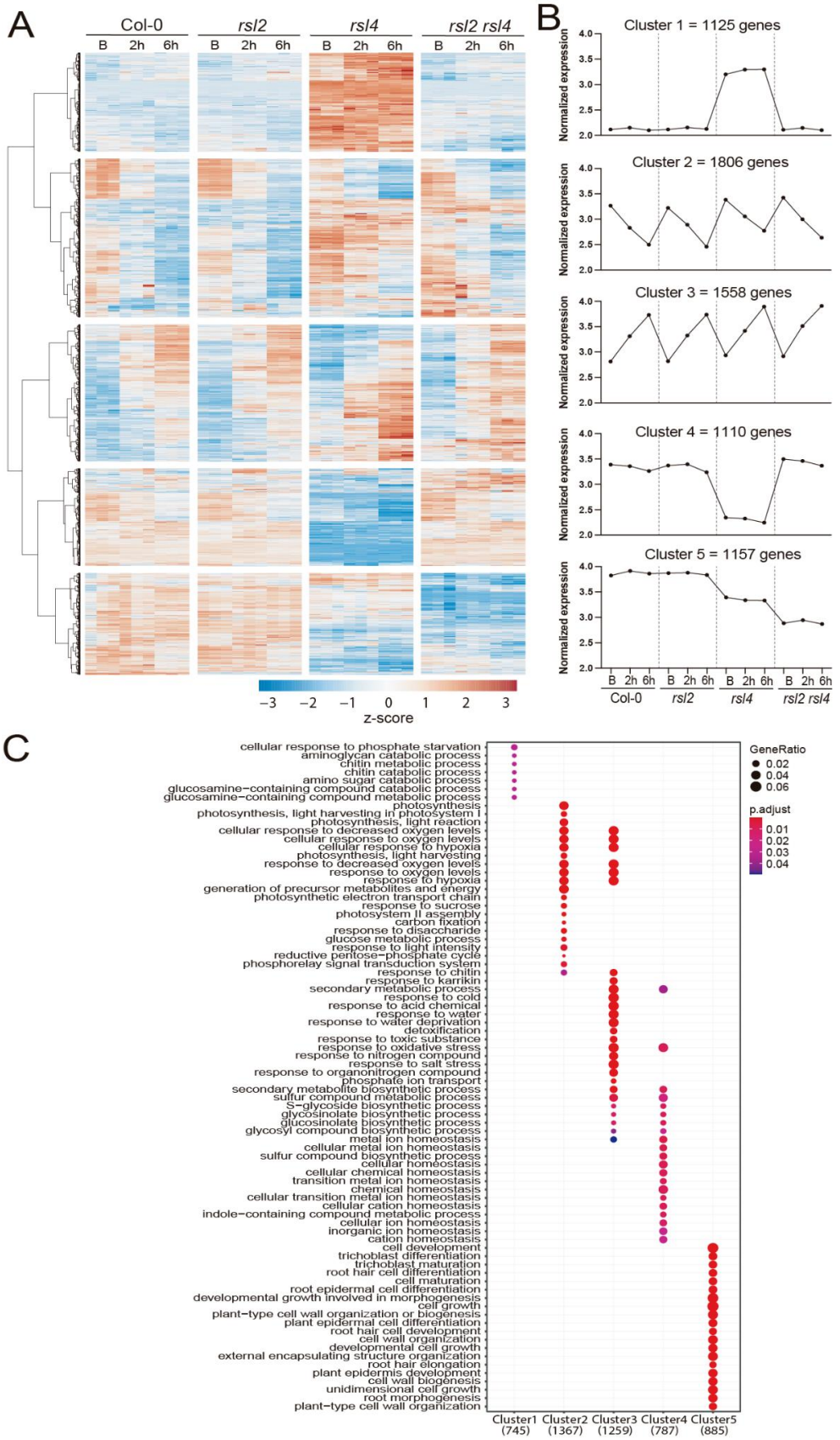

Figure S2. **DEG analysis between Col-0 and *rsl2, rsl4* and *rsl2rsl4* mutants at low temperature at 2h and 6h.** (**A**) Root samples of *Arabidopsis thaliana* cv. Col-0 were

712 compared with the mutant samples *rsl2*, *rsl4* and the double mutant *rsl2 rsl4* in a basal
713 state at 22ºC (B) and two cold treatments for 2 and 6 hours at 0ºC (2h and 6h). 6,756
714 differentially expressed genes (DEG) in at least one condition were represented in a
715 blue-red scale heatmap. Each column represents the expression of each replicate.
716 Expression data was scaled considering the mean centered divided to standard
717 deviation. (**B**) Clustering analysis of differential expressed genes was made using the
718 Ward method. Continuous line represents each cluster tendency. (**C**) Gene ontology
719 term enrichment analysis of genes belonging to each one of the identified 1-5 clusters.
720 GO in cluster 5 showed several RH development processes. The blue-red scale color
721 represents adjusted p-value and the point size represents gene ratio.
722

723

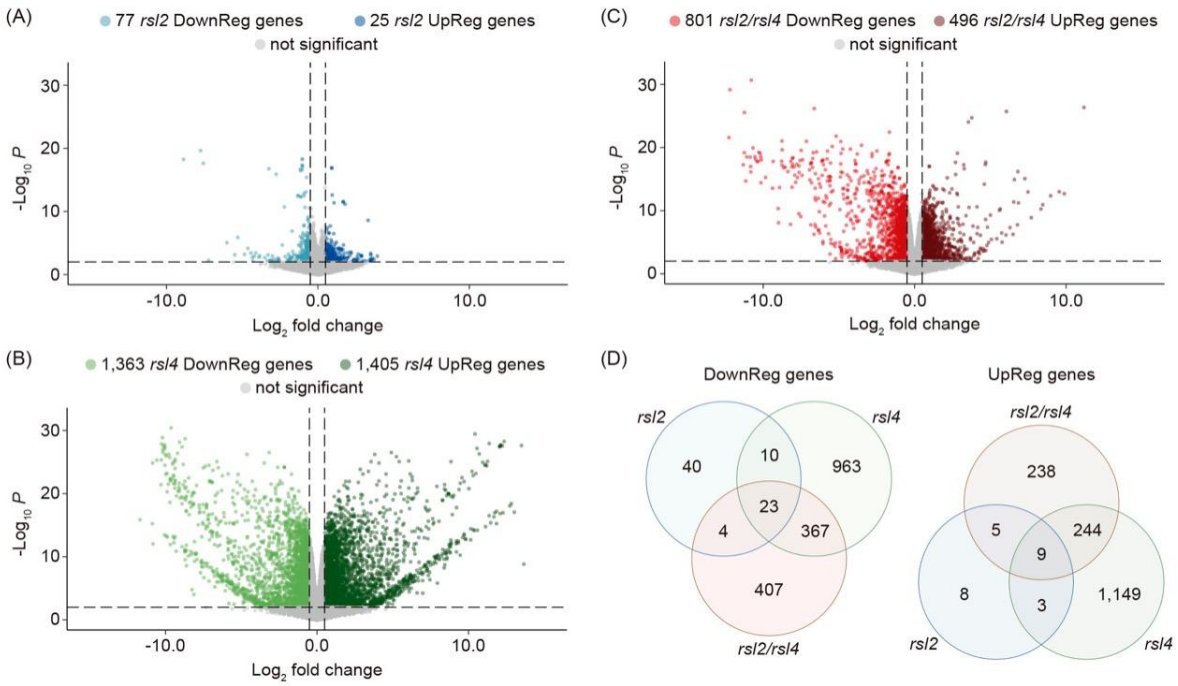

724

725

726 **Figure S3. Differential expression analysis between Col-0 and rsl2 *rsl4* mutant samples**
727 **in low temperature treatment.** (**A**) Volcano plot for differentially expressed genes
728 comparing Col-0 and *rsl2* single mutant. Candidate genes were filtered with a *p-value* <
729 0.01. Down (light blue points) and up (dark blue points) regulated *rsl2* genes were
730 selected with an FC < -0.5 and FC > 0.5, respectively. (**B**) Volcano plot for differentially
731 expressed genes comparing Col-0 and *rsl4* single mutant. Candidate genes were filtered
732 with a *p-value* < 0.01. Down (green points) and up (dark green points) regulated *rsl4*
733 genes were selected with an FC < -0.5 and FC > 0.5, respectively. (**C)** Volcano plot for
734 differentially expressed genes comparing Col-0 and *rsl2rsl4* double mutant. Candidate
735 genes were filtered with a *p-value* < 0.01. Down (red points) and up (dark red points)
736 regulated *rsl2rsl4* genes were selected with an FC < -0.5 and FC > 0.5, respectively. (**D**)
737 Venn diagram comparing the down (left side) and up (right side) regulated transcripts
738 between *rsl2, rsl4* and *rsl2rsl4* candidate genes.

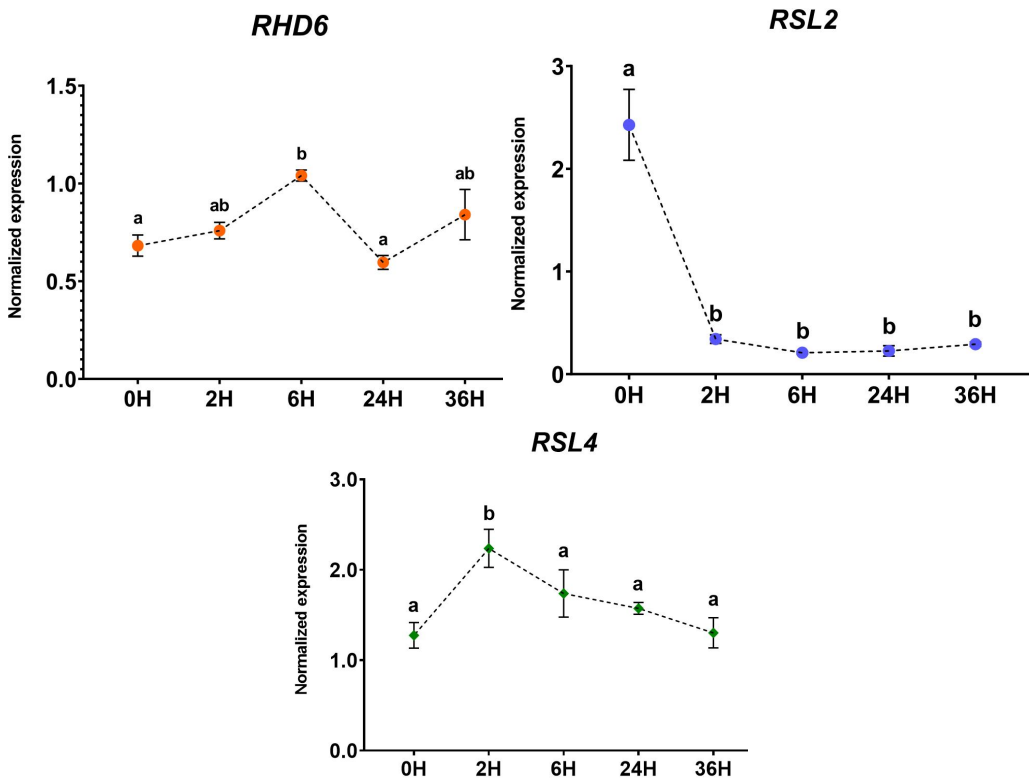

Figure S4. **Expression of *RHD6*, *RSL4* and *RSL2* under low temperature.** *RHD6, RSL2* and *RLS4* transcript levels were measured by RT-qPCR in roots of Wt Col-0 roots in parallel after 10 days at 22°C, followed by 6h, 24h and 36h at 10°C. Statistical differences between populations were assessed by one-way ANOVAs followed by Tukey post-tests. Significant differences were represented by letters. The average Cts for the technical duplicates of each transcript were normalized using the constant housekeeping transcript of *TAFII15*, which was evaluated parallelly in the same fashion. (a) $p < 0.05$, (ab) $p < 0.005$, (b) $p < 0.001$.

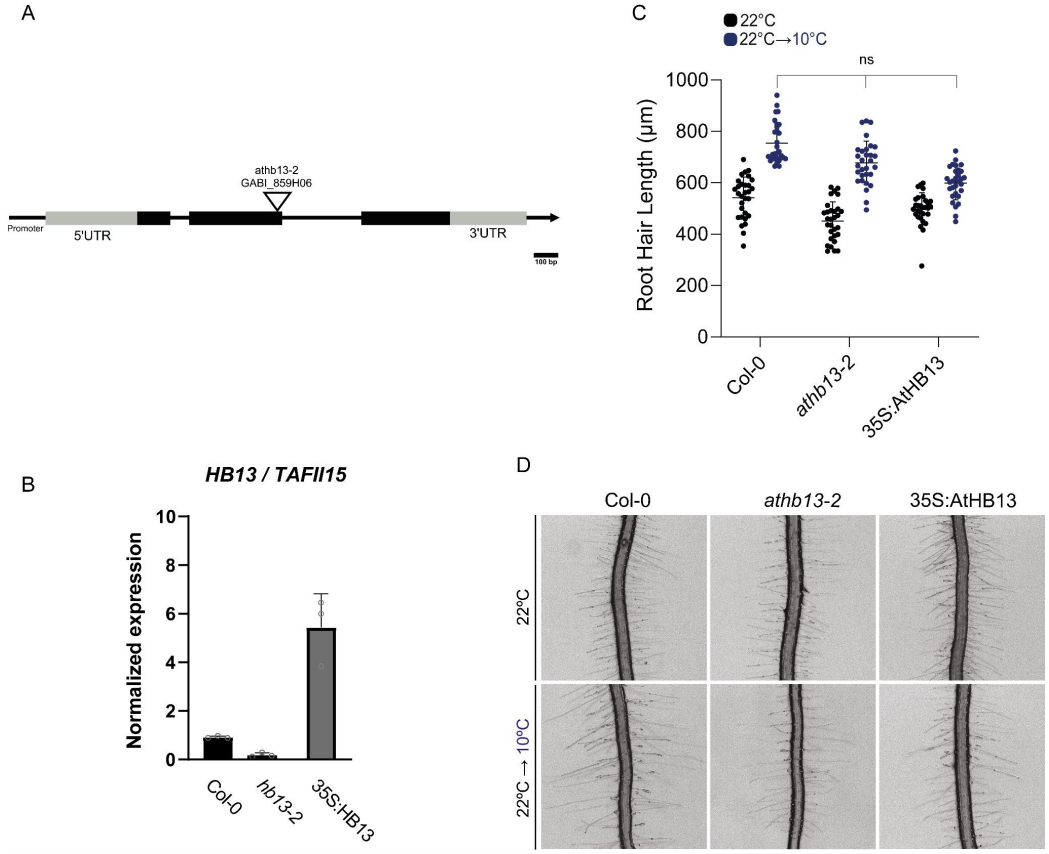

Figure S5. (**A**) AtHB13 gene structure and the insertion of the T-DNA mutants. Arrow indicates the position of the primers. (**B**) Scatter-plot of RH length of Col-0, *athb13-2* mutant and overexpressor 35S:AtHB13 grown at 22°C or at 10°C. Each point is the mean of the length of the 10 longest RHs identified in a single root. Data are the mean ± SD (N=20 roots), two-way ANOVA followed by a Tukey–Kramer test; ns=non-significant. Results are representative of three independent experiments. Asterisks indicate significant differences between Col-0 and the corresponding genotype at the same temperature. (**C**) Representative images of each genotype are shown below. Scale bars= 500 µm. (**D**) AtHB13 expression levels in Col-0, *athb13-2* and 35S:HB13 lines.

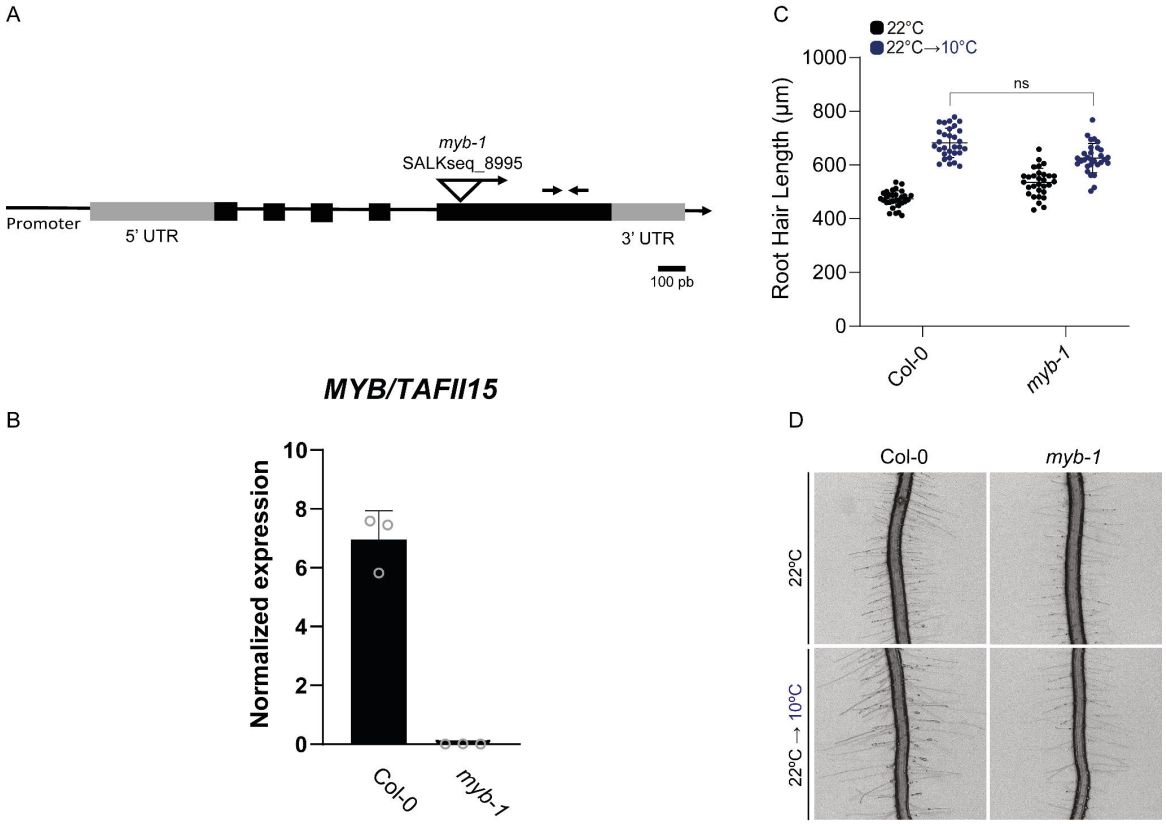

Figure S6. (**A**) MYB-like gene structure and the insertion of the T-DNA mutant. (**B**) MYB like expression levels in Col-0, *myb-like-1* line. (**C**) Scatter-plot of RH length of Col-0, mutants grown at 22°C or at 10°C. Each point is the mean of the length of the 10 longest RHs identified in a single root. Data are the mean ± SD (N=20 roots), two-way ANOVA followed by a Tukey–Kramer test; ns=non-significant. Results are representative of three independent experiments. Asterisks indicate significant differences between Col-0 and the corresponding genotype at the same temperature. (**D**) Representative images of each genotype. Scale bars= 500 µm.

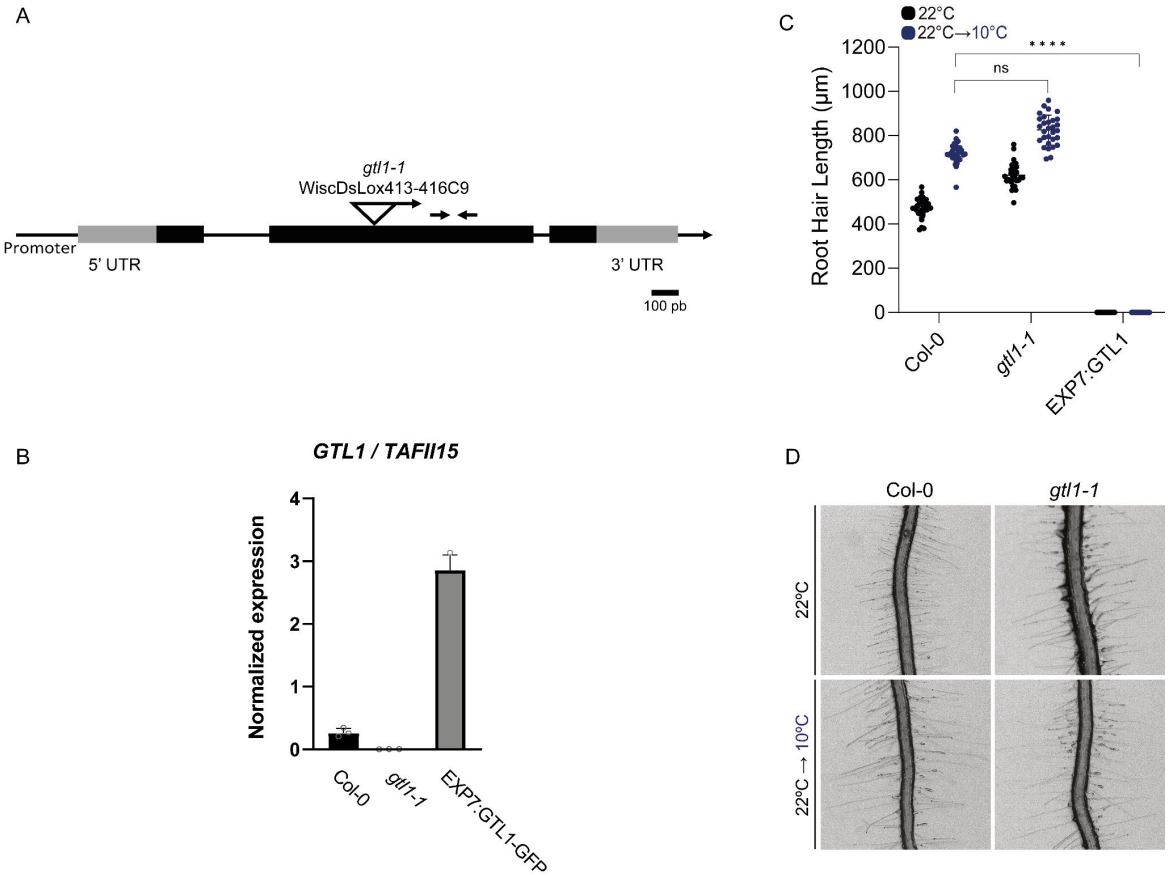

Figure S7. (**A**) GTL1 gene structure and the insertion of the T-DNA mutant *gtl1-1*. (**B**) GTL1 expression levels in Col-0, *gtl1-1* and the overexpressor EXP7:GTL1-GFP lines. (**C**) Scatter-plot of RH length of Col-0 and *gtl1-1* mutant, overexpressos EXP7:GTL1-GFP grown at 22°C or at 10°C. Each point is the mean of the length of the 10 longest RHs identified in a single root. Data are the mean ± SD (N=20 roots), two-way ANOVA followed by a Tukey–Kramer test; (***) p <0.001, NS=non-significant. Results are representative of three independent experiments. Asterisks indicate significant differences between Col-0 and the corresponding genotype at the same temperature. (**D**) Representative images of each genotype are shown below. Scale bars= 500 µm.

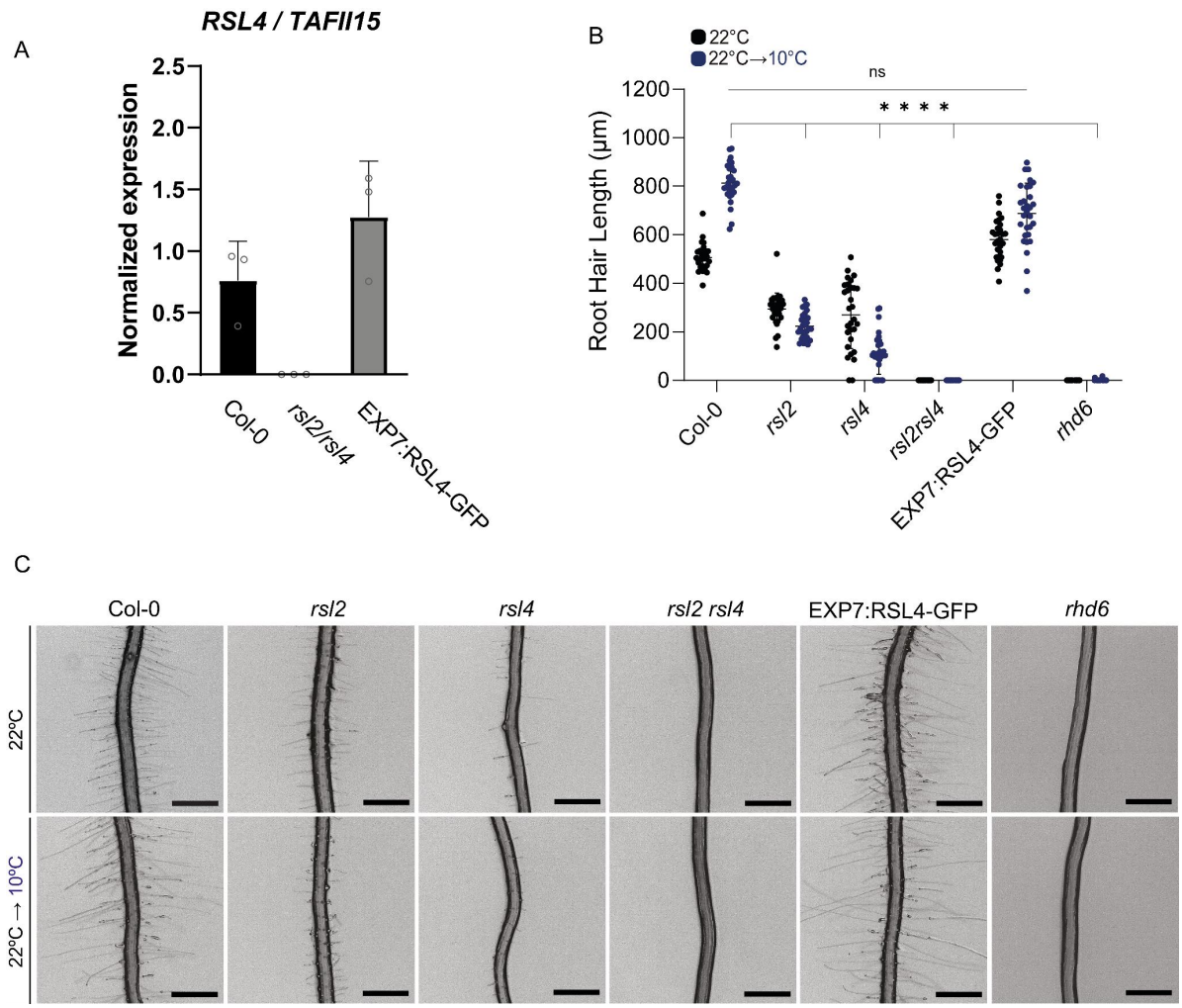

Figure S8. (**A**) RSL4 expression levels in Col-0, *rsl2/rsl4* and the overexpressor EXP7:RSL4-GFP lines (**B**) Scatter-plot of RH length of Col-0, *rsl2-1* and *rsl4-1* mutants, overexpressor EXP7:RSL4-GFP, *rhd6* grown at 22°C or at 10°C. Each point is the mean of the length of the 10 longest RHs identified in a single root. Data are the mean ± SD (N=20 roots), two-way ANOVA followed by a Tukey–Kramer test; (*) $p < 0.05$, (***) $p < 0.001$, NS=non-significant. Results are representative of three independent experiments. Asterisks indicate significant differences between Col-0 and the corresponding genotype at the same temperature. (**C**) Representative images of each genotype are shown below. Scale bars= 500 µm.

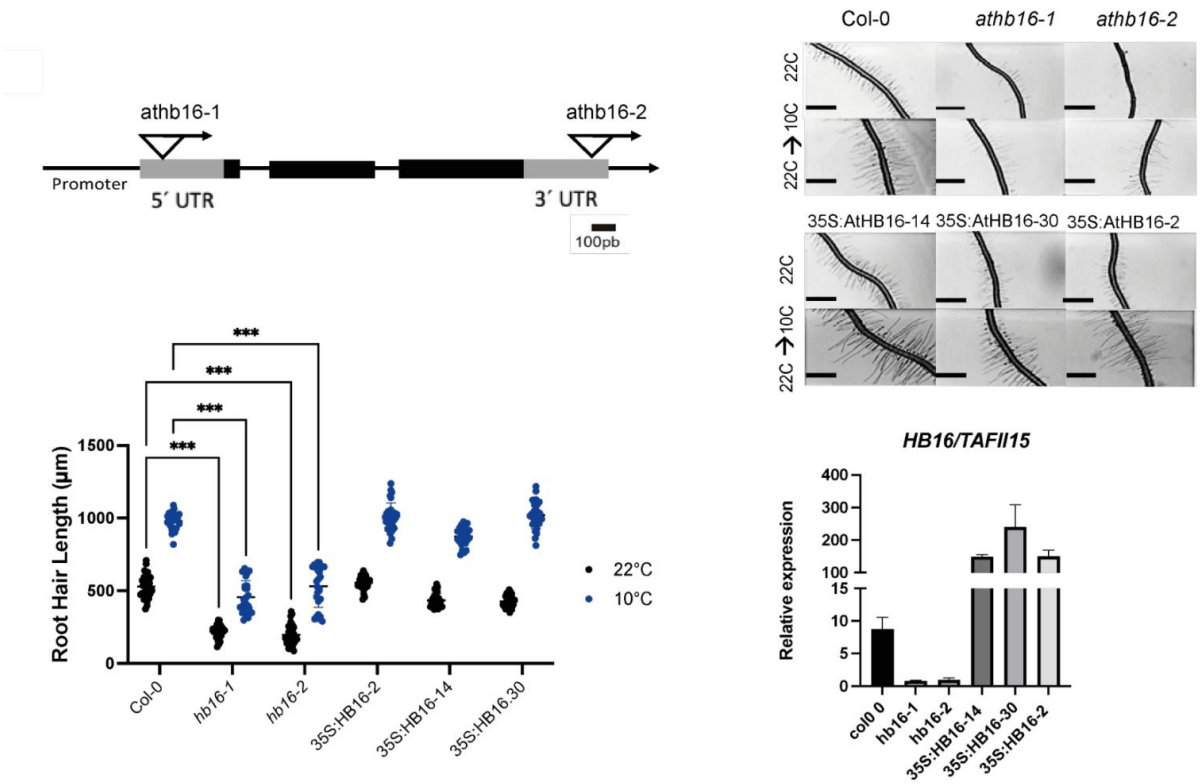

Figure S9. (**A**) AtHB16 gene structure and the insertion of the T-DNA mutants. (**B**) Scatter-plot of RH length of Col-0, *athb16-1* and *athb16-2* mutants and 35S:AtHB16 lines (2,14,30) grown at 22°C or at 10°C. Each point is the mean of the length of the 10 longest RHs identified in a single root. Data are the mean ± SD (N=20 roots), two-way ANOVA followed by a Tukey–Kramer test; (***) p <0.001, NS=non-significant. Results are representative of three independent experiments. Asterisks indicate significant differences between Col-0 and the corresponding genotype at the same temperature. (**C**) Representative images of each genotype are shown below. Scale bars= 500 µm. (**D**) AtHB13 expression levels in Col-0, *athb16-1* and *athb16-2* mutants and 35S:AtHB16 overexpression lines (2,14,30).

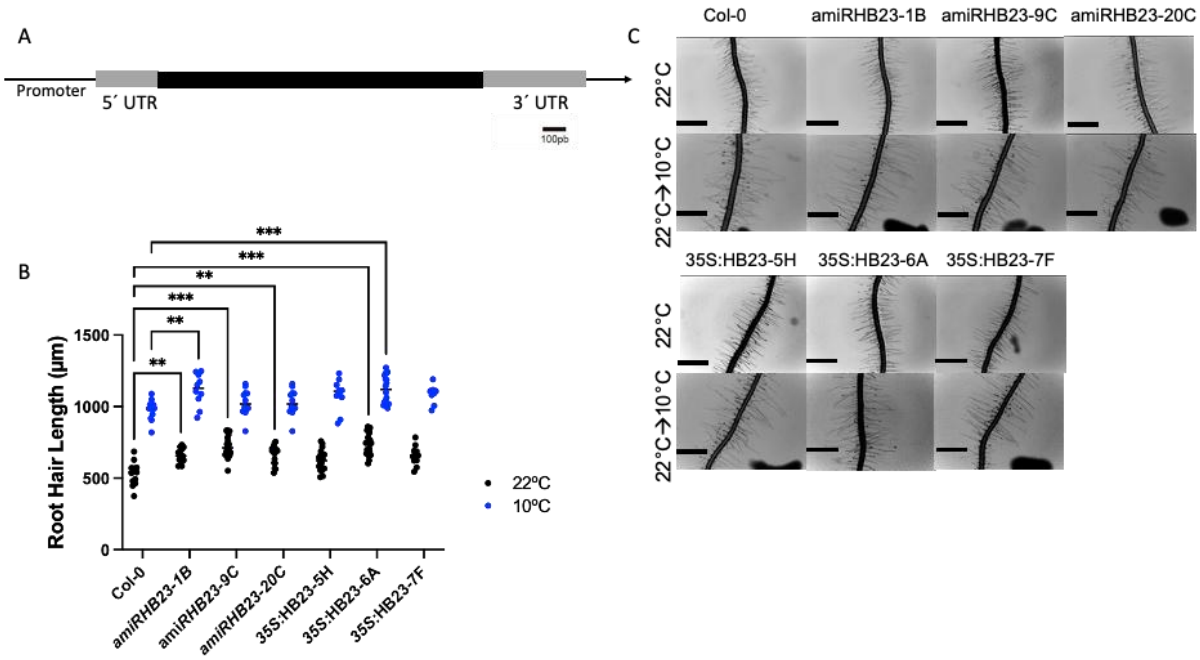

Figure S10. (**A**) AtHB23 gene structure and target of the amiRNA *athb23* silenced lines. (**B**) Scatter-plot of RH length of Col-0, amiRNA *athb23* (IB, 9C, 20C) lines and 35S:AtHB23 lines (5H, 6A,7F) grown at 22°C or at 10°C. Each point is the mean of the length of the 10 longest RHs identified in a single root. Data are the mean ± SD (N=20 roots), two-way ANOVA followed by a Tukey–Kramer test; (**) p <0.01, (***) p <0.001, NS=non-significant. Results are representative of three independent experiments. Asterisks indicate significant differences between Col-0 and the corresponding genotype at the same temperature. (**C**) Representative images of each genotype are shown below. Scale bars= 500 µm. (**D**) AtHB13 expression levels in Col-0, amiRNA *athb23-1* and amiRNA *athb23* (IB, 9C, 20C) lines and 35S:AtHB23 line.

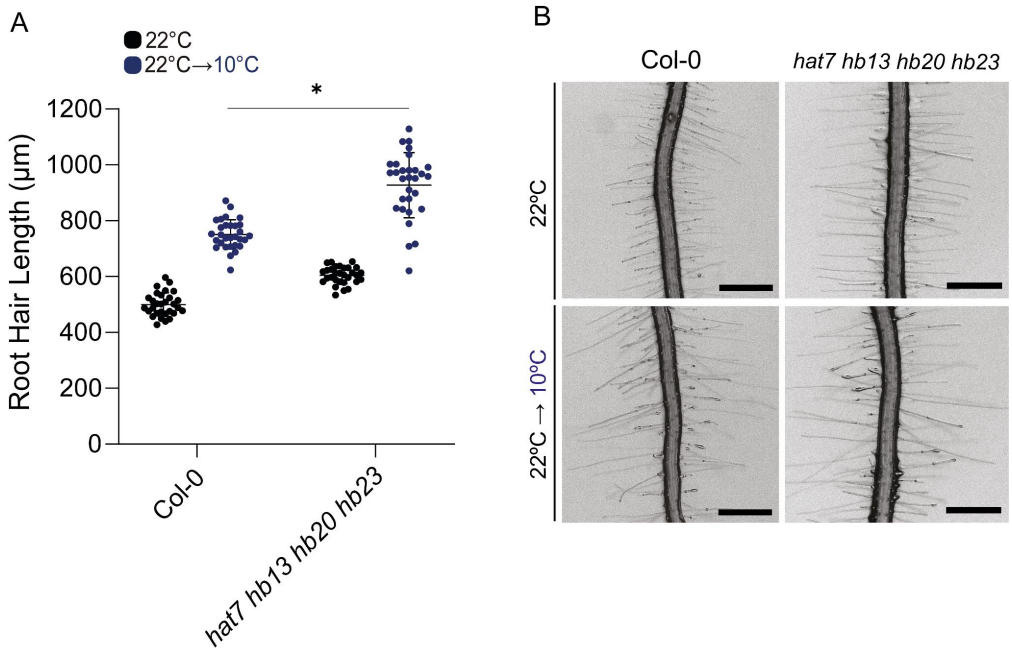

Figure S11. (**A**) Scatter-plot of RH length of Col-0, and quadruple *athb3 athb13 athb20 athb23* grown at 22°C or at 10°C. Each point is the mean of the length of the 10 longest RHs identified in a single root. Data are the mean ± SD (N=20 roots), two-way ANOVA followed by a Tukey–Kramer test; (*) $p < 0.05$. Results are representative of three independent experiments. Asterisks indicate significant differences between Col-0 and the corresponding genotype at the same temperature. (**B**) Representative images of each genotype are shown below. Scale bars= 500 µm.

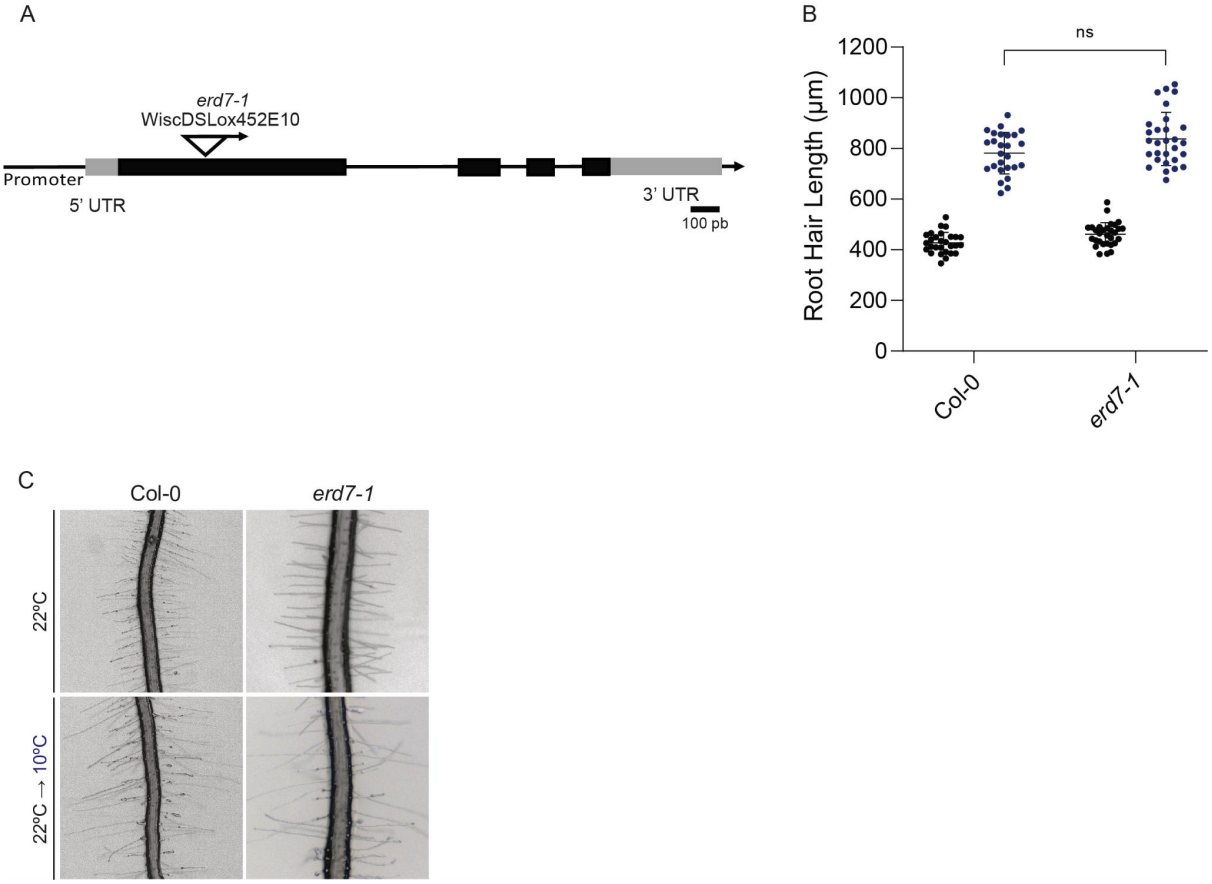

Figure S12. (**A**) ERD7 gene structure and the insertion of the T-DNA mutants. (**B**) Scatter-plot of RH length of Col-0, *erd7-1* mutant grown at 22°C or at 10°C. Each point is the mean of the length of the 10 longest RHs identified in a single root. Data are the mean ± SD (N=20 roots), two-way ANOVA followed by a Tukey–Kramer test; ns=non-significant. Results are representative of three independent experiments. Asterisks indicate significant differences between Col-0 and the corresponding genotype at the same temperature. (**C**) Representative images of each genotype are shown below. Scale bars= 500 µm.

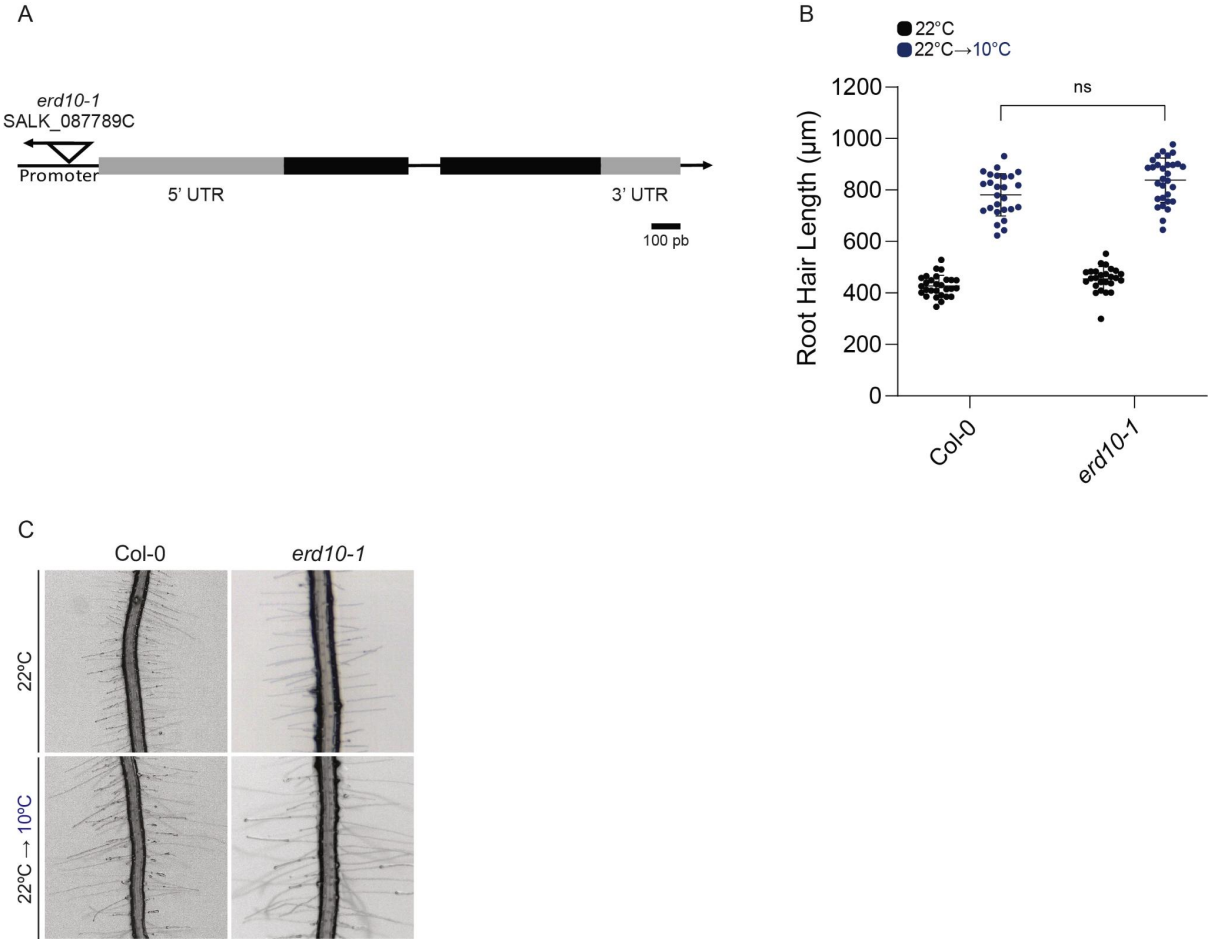

Figure S13. (**A**) ERD10 gene structure and the insertion of the T-DNA mutants. (**B**) Scatter-plot of RH length of Col-0 and *erd10-1* mutant grown at 22°C or at 10°C. Each point is the mean of the length of the 10 longest RHs identified in a single root. Data are the mean ± SD (N=20 roots), two-way ANOVA followed by a Tukey–Kramer test; ms=non-significant. Results are representative of three independent experiments. Asterisks indicate significant differences between Col-0 and the corresponding genotype at the same temperature. (**C**) Representative images of each genotype are shown below. Scale bars= 500 µm.

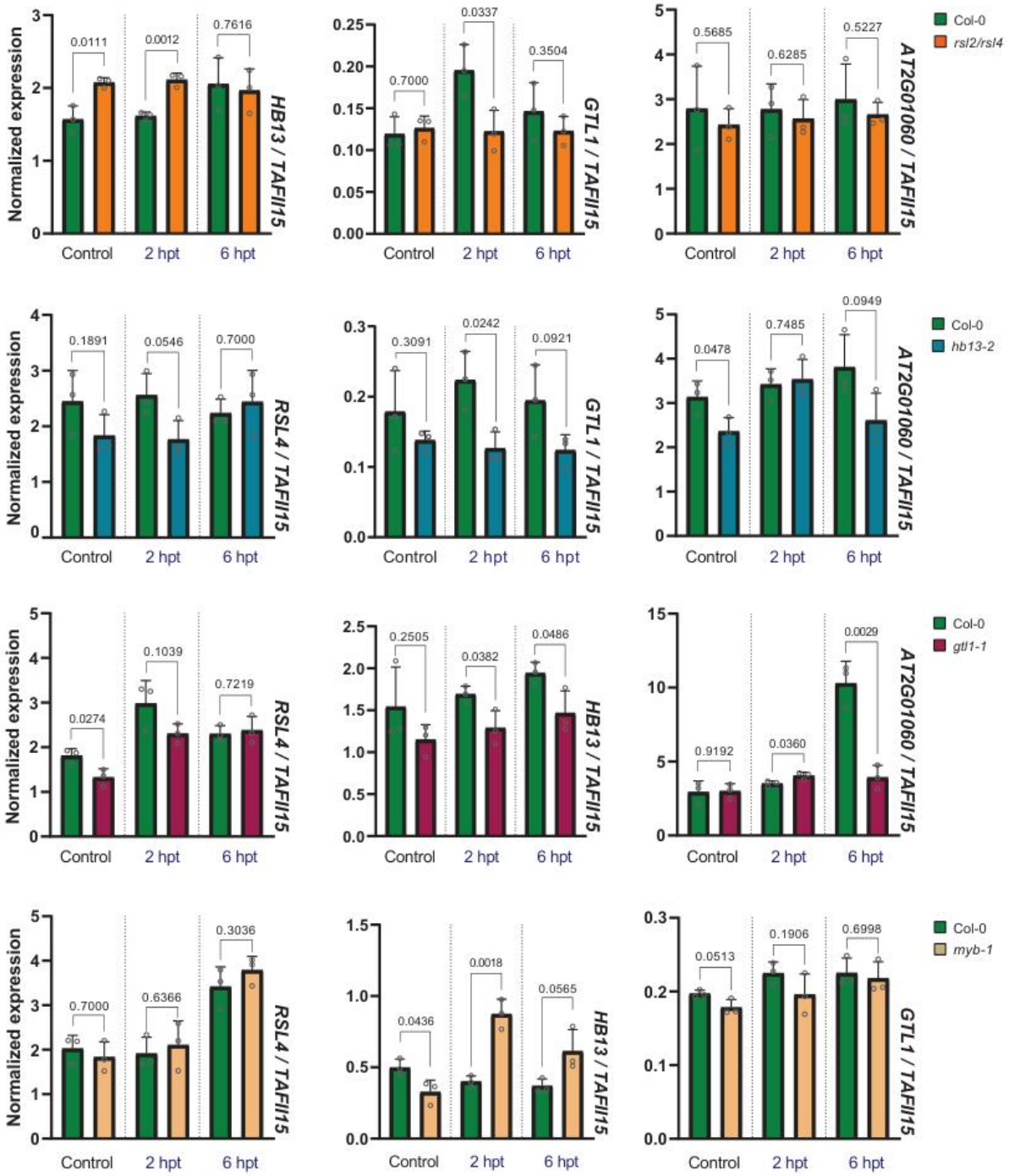

Figure S14. Expression levels of the RH main gene regulatory network nodes RSL4, AtHB13 and GTL1, and MYB-like (AT2G01060) in Wt and in the mutants *rsl2/rsl4*, *athb13-2*, *gtl1-1* and *myb-like*. The mean and standard deviation is plotted, followed by parametric and non-parametric T-tests on populations paired treatment-wise.

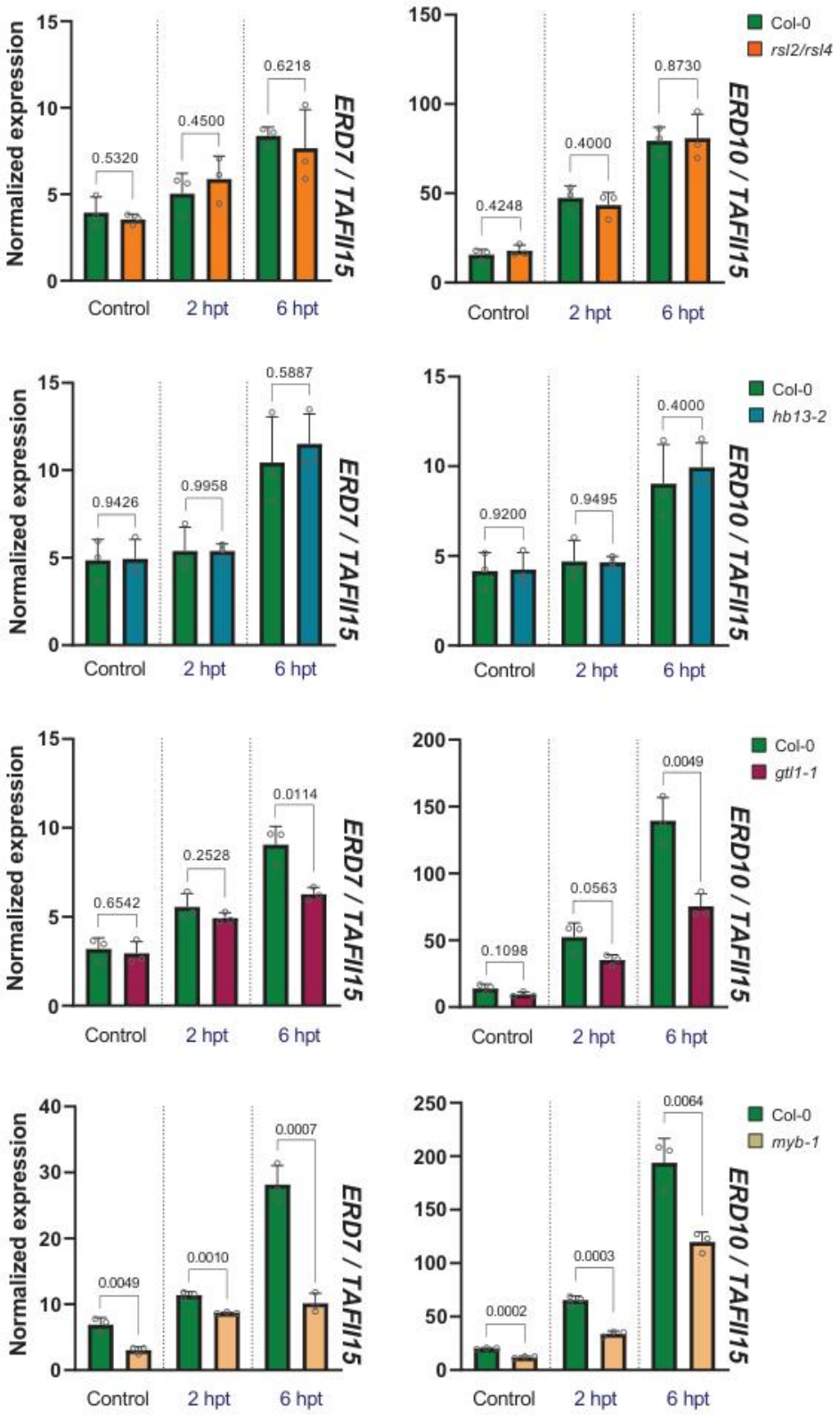

Figure S15. Expression levels of the RSL4-downstream genes ERD7 and ERD10 in Wt and in the mutants *rsl2/rsl4*, *athb13-2*, *gtl1-1* and *myb-like 1*. The mean and standard deviation is plotted, followed by parametric and non-parametric T-tests on populations paired treatment-wise.

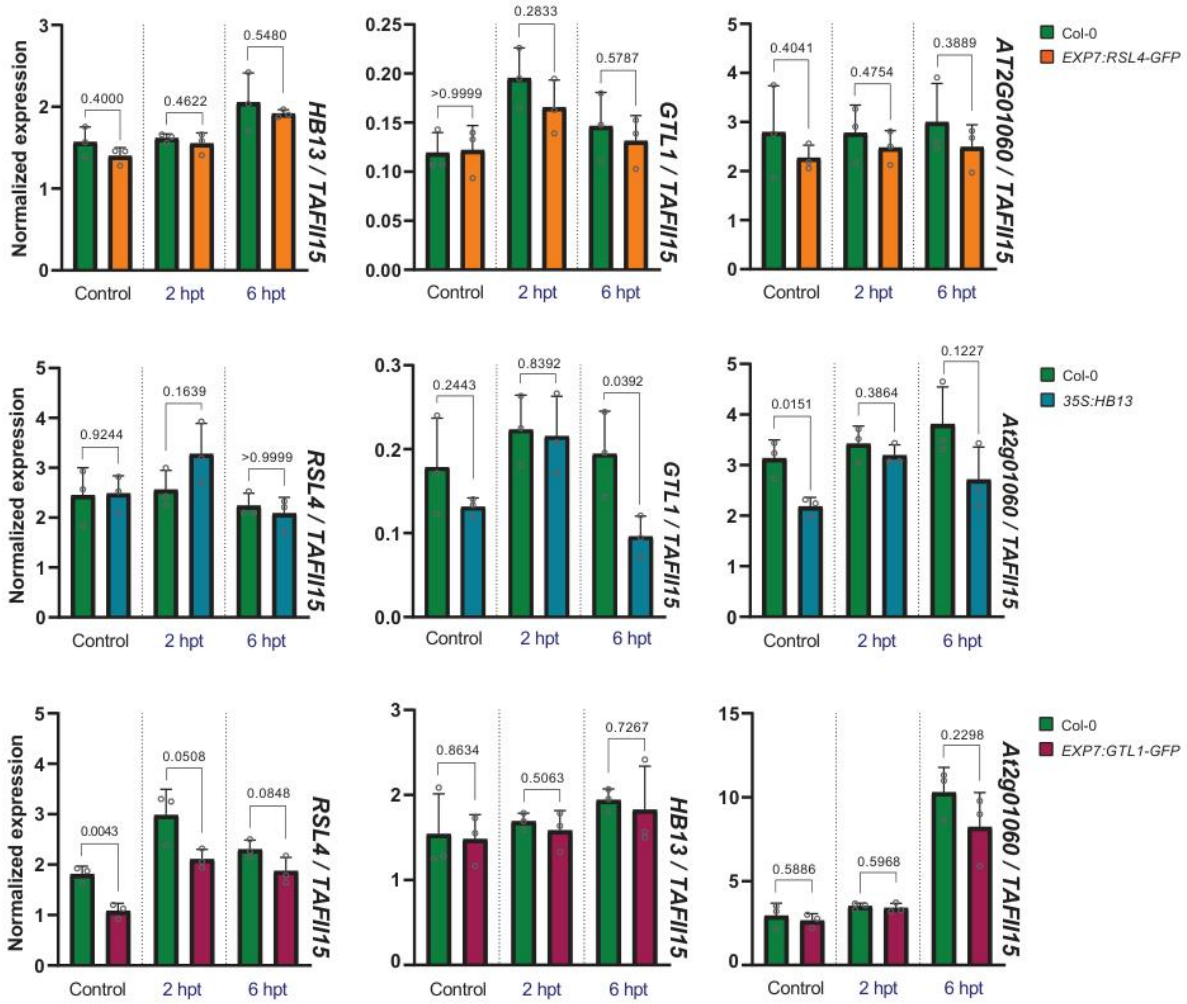

Figure S16. Expression levels of the RH main gene regulatory network nodes RSL4, AtHB13 and GTL1, and MYB-like (AT2G01060) in Wt and in the overexpression lines EXP7:RSL4-GFP, EXP7:GTL1-GFP and 35S:AtHB13. The mean and standard deviation is plotted, followed by parametric and non-parametric T-tests on populations paired treatment-wise.

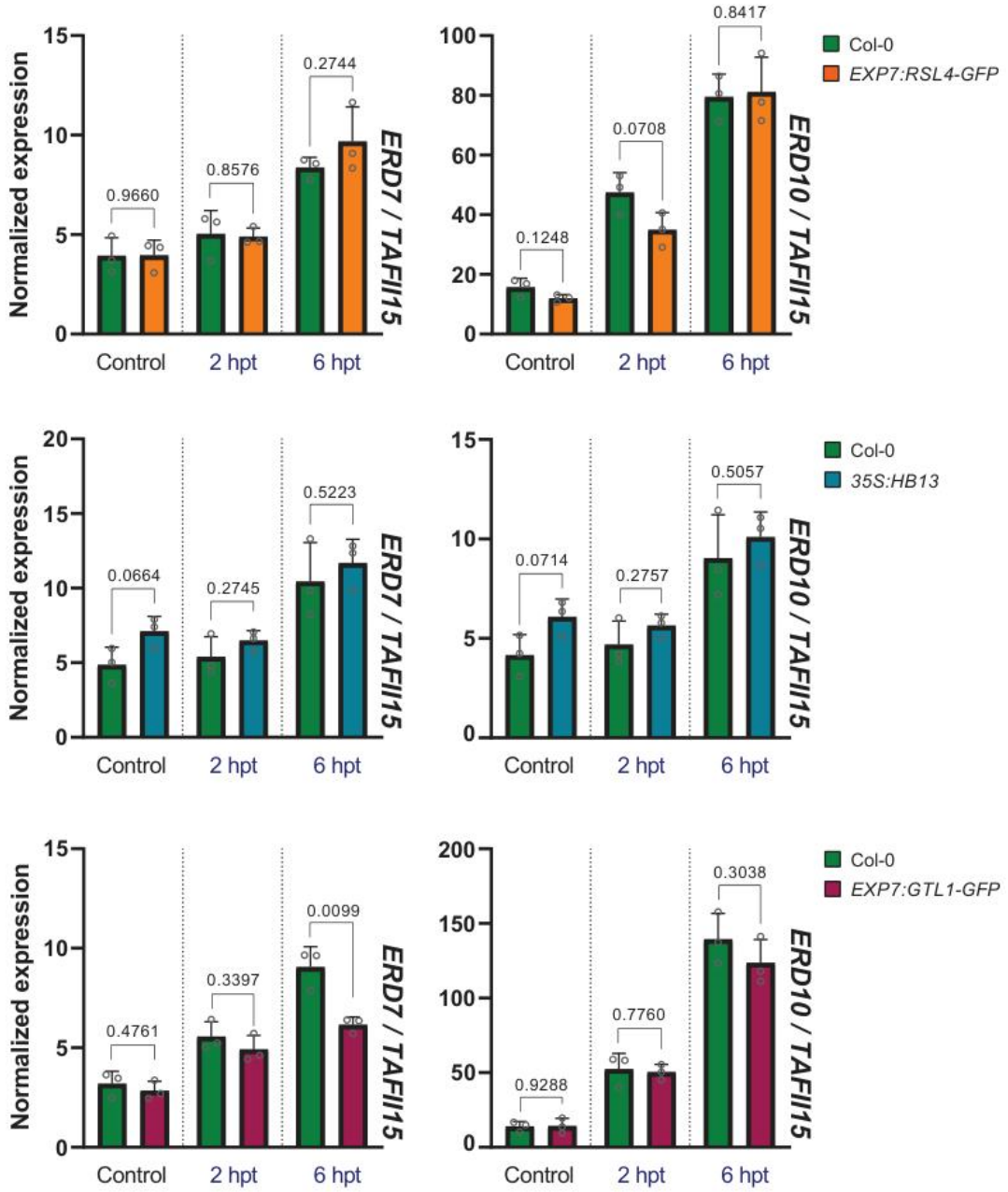

Figure S17. Expression levels of the RSL4-downstream genes ERD7 and ERD10 in Wt and in the overexpression lines EXP7:RSL4-GFP, EXP7:GTL1-GFP and 35S:AtHB13. The mean and standard deviation is plotted, followed by parametric and non-parametric T-tests on populations paired treatment-wise.

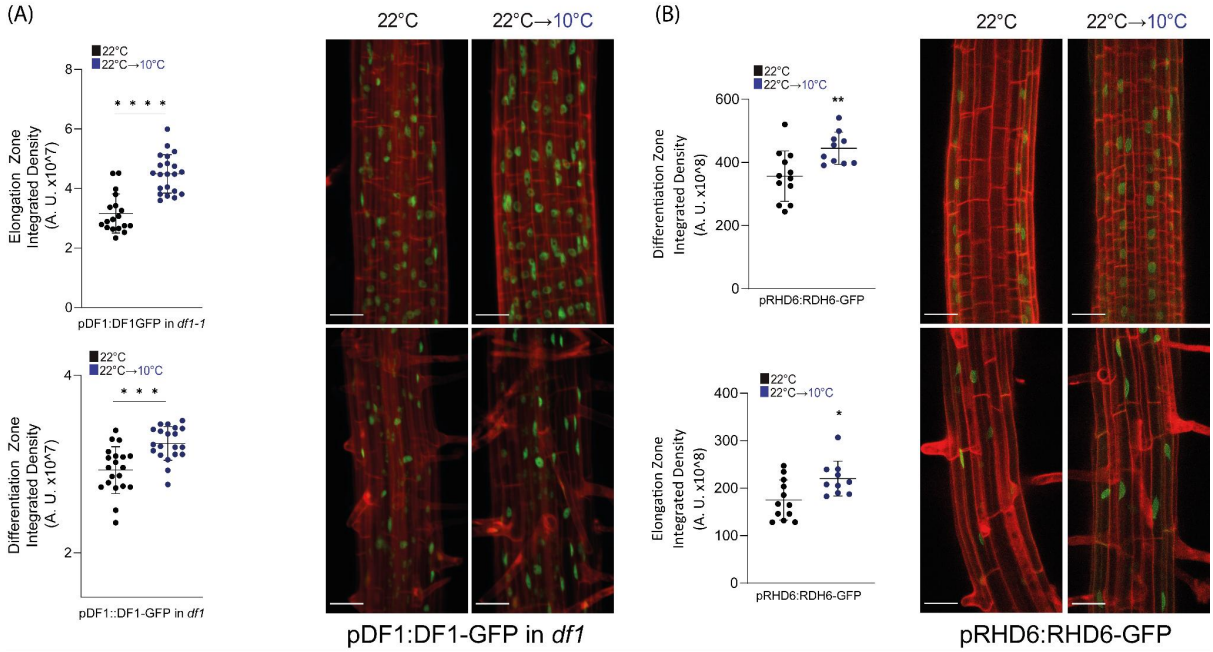

Figure S18. **Effect of the low temperature on the expression of DF1 and RHD6 in the elongation and differentiation root zones**. (**A**) Confocal images of DF1:DF1-GFP in *df1-1* translational reporter line of at 22°C and after transfer from ambient to low temperature (22°C→10°C). Quantitative evaluation of the GFP fluorescence intensity across the root elongation zones at 22°C and after transfer from ambient to low temperature. Fluorescence intensity is expressed in arbitrary units (A.U.), N=6-8 roots. Results are representative of three independent experiments. Scale bars=50 µm. (**B**) Confocal images of RHD6:RHD6-GFP translational reporter line of at 22°C and after transfer from ambient to low temperature (22°C→10°C). Quantitative evaluation of the GFP fluorescence intensity across the root elongation zones at 22°C and after transfer from ambient to low temperature. Fluorescence intensity is expressed in arbitrary units (A.U.), N=8 roots. Results are representative of three independent experiments. Scale bars=50 µm.

877 **Table S1**. Mutants and transgenic lines used and generated in this study.

878

Mutants and transgenic lines					
Locus	**Gene name**	**Gene expression effect**	**Line name**	**ABRC name/stock number**	**Reference**
AT1G27740	***RSL4***	mutant	*rsl2 rsl4*		Yi et al., 2010
		O.E.	EXP7:RSL4		Yi et al., 2010
AT1G69780	***AtHB13***	mutant	*athb13-1*	SAIL_893_G05	Ribone et al., 2015
		mutant	*athb13-2*	GABI_859H06	Ribone et al., 2015
		O.E.	35S:AtHB13		Cabello et al., 2012
		reporter GUS	HB13:GUS		Ribone et al., 2015
AT2G01060	***MYB-like***	mutant	*myb-like 1*	SALKseq_8995	this study
AT1G33240	***GTL1***	complemented	GTL1:GTL1-GFP/*gtl1-1*		Shibata et al., 2018
		O.E.	EXP7:GTL1-GFP/Col-0		Shibata et al., 2018
		mutant	*gtl1-1*	WiscDsLox413-416C9	Shibata et al., 2018
		mutant	*gtl1-1 df1-1*		Shibata et al., 2018
AT1G76880	***DF1***	complemented	DF1:DF1-GFP/*df1-1*		Shibata et al., 2018
		O.E.	EXP7:DF1-GFP/Col-0		Shibata et al., 2018
		mutant	*df1-1*	SALK_106258	Shibata et al., 2018
AT4G40060	***AtHB16***	mutant	*athb16-1*		This study
		mutant	*athb16-2*		This study
		O.E.	35S:AtHB16-2		This study
		O.E.	35S:AtHB16-14		This study
		O.E.	35S:AtHB16 30		This study
		reporter GUS	HB16:GUS		This study
AT5G39760	***AtHB23***	O.E.	35S:AtHB23-7F		Perotti et al. 2021, 2022
		O.E.	35S:AtHB23-5H		Perotti et al. 2021, 2022
		O.E.	35S:AtHB23-6A		Perotti et al. 2021, 2022
		silenced	amiR-AtHB23-1B		Perotti et al. 2021, 2022
		silenced	amiR-AtHB23-20C		Perotti et al. 2021, 2022
		silenced	amiR-AtHB23-9C		Perotti et al. 2021, 2022
		reporter GUS	HB23:GUS		Perotti et al. 2021
AT5G15150 **AT1G69780**	***AtHB3*** ***AtHB13***	mutant mutant	*Athb3 athb13 athb20*		Nolan et al. 2023

AT3G01220 **AT5G39760**	***AtHB20*** ***AtHB23***	mutant mutant	*athb23*		
AT2G17840	***ERD7***	mutant	*erd7-1*	WISCDSLOX452E10	this work
AT1G20450	***ERD10***	mutant	*erd10-1*	SALK_087789C	this work

879

880 **Table S2**. Oligonucleotide list for RT-qPCR analysis. Primer sequences along with their
881 respective Tms are shown next to their corresponding targeted genes.
882

RT-qPCR primer list		
Gene	**Primer probe**	**Sequence (5' - 3')**
AT2G01060	Forward	TCGATTGGTGAGAGGTGCAG
	Reverse	AAAGGCGAGGACATGGTCTG
ERD7	Forward	AAGGGCTCGATGCAGCAGGATA
	Reverse	GGTTTTTGCAAGCGTCGAAGGC
ERD10	Forward	ACCGATTGCTGACATCCCGGAG
	Reverse	TCTCCAGTGGTCTTGGCGTGAT
GTL1	Forward	ATGGAATTGTTTGAAGGTTTGG
	Reverse	GACATGACCTCGTGTTCTCG
AtHB13	Forward	TCTCAACTGCGCCGCCATCAAA
	Reverse	GCGACGGTGGGAAGAAGTGTCG
RHD6	Forward	TGATTTGGTGACAATGCTTGA
	Reverse	GGAGAGAATGGCATCAATGG
RSL2	Forward	CCCCAATGGAACAAAGGTC
	Reverse	TCTCGGTGAGCTGAGACCAA
RSL4	Forward	GTGCCAAACGGGACAAAAGT
	Reverse	TTGTGATGGAACCCCATGTC
TAFII15	Forward	GAATCACGGCCAACAATC
	Reverse	ACTCTTAGCCAAGTAGTGCTCC

Genotyping primer list		
Gene	**Primer probe**	**Sequence (5' - 3')**
myb-1 **(SALKseq_8995.3)**	Left primer	CCATGAGAGGGAAAGCCTATC
	Right primer	AGGACATGGTCTGACTGATGG
myb-2 **(SALKseq_034222)**	Left primer	AGGAGCAATTTGAACTCCCTC
	Right primer	TTGGAAACCTGGATTGTTGAC
erd7-1 **(WISCDSLOX452E10)**	Left primer	TTTAATGCAATTTCCGAGACG
	Right primer	CAATCTCTTTCCTTTCCCCAG
erd10-1 **(SALK_087789C)**	Left primer	CTCACCGTCTTCACCTTCTTC
	Right primer	TGCATTCTTCTCCAATTCTCC

883

884 **REFERENCES**

885

886 M.K. Aalto, E. Helenius, T. Kariola, V. Pennanen, P. Heino, H. Horak, I. Puzorjova,H.
887 Kollist, E.T. Palva, ERD15-An attenuator of plant ABA responses and stomatal aperture,
888 Plant Sci. 182 19–28. https://doi.org/10.1016/j.plantsci.2011.08.009 (2012).

889

890 Alvarez, J. M., Riveras, E., Vidal, E. A., Gras, D. E., Contreras-López, O., Tamayo, K. P.,
891 Aceituno, F., Gómez, I., Ruffel, S., Lejay, L., Jordana, X., Gutiérrez, R. A. Systems
892 approach identifies TGA1 and TGA4 transcription factors as important regulatory
893 components of the nitrate response of Arabidopsis thaliana roots. *Plant J*. 80(1), 1-13
894 https://doi.org/10.1111/tpj.12618 (2014).

895

896 Arce, A.L., Raineri, J., Capella, M., Cabello, J.V. , Chan, R.L. Uncharacterized conserved
897 motifs outside the HD-Zip domain in HD-Zip subfamily I transcription factors; a potential
898 source of functional diversity. *BMC Plant Biol.* 11(42). http://doi.org/10.1186/1471-
899 2229-11-42 (2011).

900

901 Ariel, F., Lucero, L., Christ, A., Mammarella, M. F., Jegu, T., Veluchamy, A., Mariappan, K.,
902 Latrasse, D., Blein, T., Liu, C., Benhamed, M., Crespi, M. R-Loop Mediated trans Action of
903 the APOLO Long Noncoding RNA. *Mol. Cell* 77(5), 1055-1065.
904 https://doi.org/10.1016/j.molcel.2019.12.015 (2020).

905

906 Barajas-Lopez JD, Tiwari A, Zarza X, Shaw MW, Pascual JS, Punkkinen M, Bakowska JC,
907 Munnik T, Fujii H. EARLY RESPONSE TO DEHYDRATION 7 Remodels Cell Membrane Lipid
908 Composition during Cold Stress in Arabidopsis. Plant Cell Physiol. 2021 Mar 25;62(1):80-
909 91. doi: 10.1093/pcp/pcaa139.

910

911 Bhosale, R., Giri, J., Pandey, B.K. *et al*. A mechanistic framework for auxin dependent
912 Arabidopsis root hair elongation to low external phosphate. *Nat. Commun.* 9, 1409.
913 https://doi.org/10.1038/s41467-018-03851-3 (2018).

914

915 Brady, S., Orlando, D., Lee, J. Y., Wang, J., Koch, J., Dinneny, J., Mace, D., Ohler, U.,
916 Benfey, P. A High-Resolution Root Spatiotemporal Map Reveals Dominant Expression
917 Patterns. *Science* 318(5851), 801-806. http://doi.org/10.1126/science.1146265 (2007).

918

919 Brooks, M., Juang, C., Katar,i M., Alvarez, J., Pasquino, A., Shih, H., Huang, J., Shanks, C.,
920 Cirrone, J., Coruzzi, G. ConnecTF: A platform to integrate transcription factor-gene
921 interactions and validate regulatory networks. *Plant Physiol.* 185(1), 49-66.
922 http://doi.org/10.1093/plphys/kiaa012 (2021).

923

924 Cabello, J. V., Arce, A. L., Chan, R. L. The homologous HD-Zip I transcription factors
925 HaHB1 and AtHB13 confer cold tolerance via the induction of pathogenesis related and
926 glucanase proteins. *Plant J.* 69(1), 141-153. http://doi.org/10.1111/j.1365-
927 313X.2011.04778.x (2012).
928
929 Capella, M., Ribone, P. A., Arce, A. L., Chan, R. L. Arabidopsis thaliana HomeoBox 1
930 (AtHB1), a homedomain-leucine zipper I (HD-Zip I) transcription factor, is regulated by
931 phytochrome-interacting factor 1 to promote hypocotyl elongation. *New Phytol.* 207(3),
932 669-682. http://doi.org/10.1111/nph.13401 (2015).
933
934 Casal, J. J., Estevez, J. M. Auxin–environment integration in growth responses to forage
935 for resources. *CSH Perspect. Biol*. 13(4), a040030.
936 http://doi.org/10.1101/cshperspect.a040030 (2021).
937
938 Cheng, M., Liao, P., Kuo, W., and Lin, T. (2013). The Arabidopsis ETHYLENE RESPONSE
939 FACTOR1 regulates abiotic stress-responsive gene expression by binding to different cis-
940 acting elements in response to different stress signals. Plant Physiol. 162, 1566–1582.
941 doi: 10.1104/pp.113.221911
942
943 Choi H., Jeong S., Kim D. S., Na H. J., Ryu J. S., Lee S. S., Nam H. G., Lim P. O., Woo H. R.
944 The homeodomain-leucine zipper ATHB23, a phytochrome B-interacting protein, is
945 important for phytochrome B-mediated red light signaling. *Plant Physiol.* 150(2), 308-
946 320. http://doi.org/10.1111/ppl.12087 (2014).
947
948 Datta, S., Prescott, H., Dolan, L. Intensity of a pulse of RSL4 transcription factor
949 synthesis determines Arabidopsis root hair cell size. *Nat. Plants* 1(15138), 1–6.
950 https://doi.org/10.1038/nplants.2015.138 (2015).
951
952 Denyer, T., Ma, X., Klesen, S., Scacchi, E., Nieselt, K., Timmermans, M. Spatiotemporal
953 Developmental Trajectories in the Arabidopsis Root Revealed Using High-Throughput
954 Single-Cell RNA Sequencing. *Dev. Cell* 48(6), 840-852.
955 https://doi.org/10.1016/j.devcel.2019.02.022 (2019).
956
957 Dodt, M., Roehr, J. T., Ahmed, R., Dieterich, C. FLEXBAR—Flexible Barcode and Adapter
958 Processing for Next-Generation Sequencing Platforms. *Biology* 1(3), 895-905.
959 https://doi.org/10.3390/biology1030895 (2012).
960
961 Doner NM, Seay D, Mehling M, Sun S, Gidda SK, Schmitt K, Braus GH, Ischebeck T,
962 Chapman KD, Dyer JM, Mullen RT. *Arabidopsis thaliana* EARLY RESPONSIVE TO
963 DEHYDRATION 7 Localizes to Lipid Droplets via Its Senescence Domain. Front Plant Sci.
964 2021 Apr 14;12:658961. doi: 10.3389/fpls.2021.658961.

965
966 Gao, D., Appiano, M., Huibers, R. P., Chen, X., Loonen, A. E. H. M., Visser, R. G. F.,
967 Wolters, B. Y. Activation tagging of ATHB13 in Arabidopsis thaliana confers broad-
968 spectrum disease resistance, *Plant Mol. Biol.* 86(6), 641-653.
969 https://doi.org/10.1007/s11103-014-0253-2 (2014).
970
971 Haling, R. E., Brown, L. K., Bengough, A.G., Young, I. M., Hallett, P. D., White, P. J.,
972 George, T. S. Root hairs improve root penetration, root–soil con tact, and phosphorus
973 acquisition in soils of different strength. *J. Exp. Bot.* 64(12), 3711–3721.
974 https://doi.org/10.1093/jxb/ert200 (2013).
975
976 Han, H., Wang, H., Han, Y., Hu, Z., Xin, M., Peng, H., Yao, Y., Sun, Q., Ni, Z. Altered
977 expression of the *TaRSL2* gene contributed to variation in root hair length during
978 allopolyploid wheat evolution. *Planta* 246(5), 1019–1028.
979 https://doi.org/10.1007/s00425-017-2735-3 (2017).
980
981 Han, Y., Xin, M., Huang, K., Yuyun, X., Zhenshan, L., Zhaorong, H., Yingyin, Y., Huiru, P.,
982 Zhongfu, N., Qixin, S. Altered expression of *TaRSL4* gene by genome interplay shapes
983 root hair length in allopolyploid wheat. *New Phytol.* 209(2), 721-732.
984 https://doi.org/10.1111/nph.13615 (2016).
985
986 Hanson, J., Regan, S., Engstrom, P. The expression pattern of the homeobox gene
987 ATHB13 reveals a conservation of transcriptional regulatory mechanisms between
988 Arabidopsis and hybrid aspen. *Plant Cell Rep*. 21(1), 81-89.
989 https://doi.org/10.1007/s00299-002-0476-6 (2002).
990
991 Henriksson, E., Olsson, A. S. B., Johannesson, H., Johansson, H., Hanson, J., Engström, P.,
992 Söderman, E. Homeodomain leucine zipper class I genes in Arabidopsis. Expression
993 patterns and phylogenetic relationships. *Plant Physiol*. 139(1), 509–518.
994 https://doi.org/10.1104/pp.105.063461 (2005).
995
996 Hwang, Y., Choi, H. S., Cho, H. M., & Cho, H. T. Tracheophytes contain conserved
997 orthologs of a basic helix-loop-helix transcription factor that modulate ROOT HAIR
998 SPECIFIC genes. *Plant Cell* 29(1), 39–53. https://doi.org/10.1105/tpc.16.00732 (2017).
999
1000 Jia, Z., Giehl, R. F. H., Hartmann, A., Estevez, J. M., Bennett, M. J., von Wiren, N. A
1001 spatially concerted epidermal auxin signaling framework steers the root hair foraging
1002 response under low nitrogen. *Curr. Biol.* 33(18), 3926–3941.
1003 https://doi.org/10.1016/j.cub.2023.08.040 (2023).
1004

1005 Jean-Baptiste, K., McFaline-Figueroa, J. L., Alexandre, C., Dorrity, M., Saunders, L., Bubb,
1006 K., Trapnell, C., Fields, S., Queitsch, C., Cuperus, J. Dynamics of Gene Expression in
1007 Single Root Cells of Arabidopsis thaliana. *Plant Cell* 31(5), 993–1011,
1008 https://doi.org/10.1105/tpc.18.00785 (2019).
1009
1010 Kim, C. M., Dolan, L. ROOT HAIR DEFECTIVE SIX-LIKE class I genes promote root hair
1011 development in the grass *Brachypodium distachyon*. *PLoS Genet.* 12(12), e1006480.
1012 https://doi.org/10.1371/journal.pgen.1006211 (2016).
1013
1014 Liao, Y., Smyth, G. K., Shi, W. The R package Rsubread is easier, faster, cheaper and
1015 better for alignment and quantification of RNA sequencing reads. *Nucleic Acids Res*.
1016 47(8). e47. https://doi.org/10.1093/nar/gkz114 (2019).
1017
1018 Lin, Q., Ohashi, Y., Kato, M., Tsuge, T., Gu, H., Qu, L. J., & Aoyama, T. GLABRA2 directly
1019 suppresses basic helix-loop-helix transcription factor genes with diverse functions in
1020 root hair development. *Plant Cell 27*(10), 2894–2906.
1021 https://doi.org/10.1105/tpc.15.00607 (2015).
1022
1023 Lopez, L. E., Chuah Y. S., Encina, F., Carignani-Sardoy M., Berdion-Gabarain, V., Mutwil,
1024 M., Estevez, J. M. New molecular components that regulate the transcriptional hub in
1025 root hairs: coupling environmental signals with endogenous hormones to coordinate
1026 growth. *J. Exp. Bot*. erad419. https://doi.org/10.1093/jxb/erad419 (2023).
1027
1028 Maher, K. A., Bajic, M., Kajala, K., Reynoso, M., Pauluzzi, G., West, D. A., Zumstein, K.,
1029 Woodhouse, M., Bubb, K., Dorrity, M. W., Queitsch, C., Bailey-Serres, J., Sinha, N., Brady,
1030 S. M., Deal, R. B. Profiling of Accessible Chromatin Regions across Multiple Plant Species
1031 and Cell Types Reveals Common Gene Regulatory Principles and New Control Modules.
1032 *Plant Cell* 30(1), 15–36. https://doi.org/10.1105/tpc.17.00581 (2018).
1033
1034 Mangano, S., Denita-Juarez, S. P., Choi, H. S., Marzol, E., Hwang, Y., Ranocha, P.,
1035 Velasquez, S. M., Borassi, C., Barberini, M. L., Aptekmann, A. A., Muschietti, J. P., Nadra,
1036 A. D., Dunand, C., Cho, H. T., & Estevez, J. M. Molecular link between auxin and ROS-
1037 mediated polar growth. *Proc. Natl. Acad. Sci. U.S.A. 114*(20), 5289–5294.
1038 https://doi.org/10.1073/pnas.1701536114 (2017).
1039
1040 Martínez-Pacheco, J., Song L., Kuběnová, L., Ovečka, M., Berdion-Gabarain, V., Peralta J.
1041 M., Urzúa-Lehuedé, T., Ibeas, M. A., Ricardi, M. M., Zhu, S., Shen, Y., Schepetilnikov, M.,
1042 Ryabova, L. A., Alvarez, J. M., Gutierrez, R. A., Grossmann, G., Šamaj, J., Yu, F., Estevez J.
1043 M. Cell surface receptor kinase FERONIA linked to nutrient sensor TORC signaling
1044 controls root hair growth at low temperature linked to low nitrate in Arabidopsis
1045 thaliana. *New Phytol*. 238(1), 169-185.https://doi.org/10.1111/nph.18723 (2023).

1046
1047 Martínez-Pacheco, J., Ranocha, P., Kasulin, L., Fusari, C. M., Servi, L., Aptekmann, A. A.,
1048 Berdion-Gabarain, V., Peralta J. M., Borassi, C., Marzol, E., Rodríguez-Garcia D. R.,
1049 Rondón-Guerrero, Y. C., Carignani-Sardoy, M., Ferrero, L., Botto, J. F., Meneses, C., Ariel,
1050 F., Nadra, A. D., Petrillo, E., Dunand C., Estevez J.M. Apoplastic class III peroxidases
1051 PRX62 and PRX69 promote Arabidopsis root hair growth at low temperature. *Nat.*
1052 *Commun.* 13(1), 1310. https://doi.org/10.1038/s41467-022-28833-4 (2022).
1053
1054 Martínez Pacheco, J., Mansilla, N., Moison, M., Lucero, L., Berdion-Gabarain, V., Ariel, F.,
1055 & Estevez, J. M. The lncRNA APOLO and the transcription factor WRKY42 target
1056 common cell wall EXTENSIN encoding genes to trigger root hair cell elongation. *Plant*
1057 *Signal. Behav.* 16(8), 1920191. https://doi.org/10.1080/15592324.2021.1920191 (2021).
1058
1059 Menand, B., Yi, K., Jouannic, S., Hoffmann, L., Ryan, E., Linstead, P., Schaefer, D. G.,
1060 Dolan, L. An ancient mechanism controls the development of cells with a rooting
1061 function in land plants. *Science* 316(5830), 1477–1480.
1062 https://doi.org/10.1126/science.1142618 (2007).
1063
1064 Miguel, M. A., Postma, J. A., Lynch, J. P. Phene synergism between root hair length and
1065 basal root growth angle for phosphorus acquisition. *Plant Physiol* 167(4), 1430–1439.
1066 https://doi.org/10.1104/pp.15.00145 (2015).
1067
1068 Moison, M., Pacheco, J. M., Lucero, L., Fonouni-Farde, C., Rodríguez-Melo, J., Mansilla,
1069 N., Christ, A., Bazin, J., Benhamed, M., Ibañez, F., Crespi, M., Estevez, J. M., & Ariel, F.
1070 The lncRNA APOLO interacts with the transcription factor WRKY42 to trigger root hair
1071 cell expansion in response to cold. *Mol. Plant* 14(6), 937-948.
1072 https://doi.org/10.1016/j.molp.2021.03.008 (2021).
1073
1074 Moon, S., Cho, L. H., Kim, Y. J., *et al*. RSL Class II transcription factors guide the nuclear
1075 localization of RHL1 to regulate root hair development. *Plant Physiol* 179(2), 558–568.
1076 https://doi.org/10.1104/pp.18.01002 (2019).
1077
1078 Nolan TM, Vukašinović N, Hsu CW, Zhang J, Vanhoutte I, Shahan R, Taylor IW,
1079 Greenstreet L, Heitz M, Afanassiev A, Wang P, Szekely P, Brosnan A, Yin Y, Schiebinger G,
1080 Ohler U, Russinova E, Benfey PN. Brassinosteroid gene regulatory networks at cellular
1081 resolution in the *Arabidopsis* root. Science. 2023 Mar 31;379(6639):eadf4721. doi:
1082 10.1126/science.adf4721.
1083
1084 O'Malley, R. C., Shao-shan, C. H., Liang, S., Mathew, G. L., Bartlett, A., Nery, J. R., Galli,
1085 M., Gallavotti, A., Ecker J. R. Cistrome and Epicistrome Features Shape the Regulatory

1086 DNA Landscape. *Cell* 165(5), 1280-1292. http://dx.doi.org/10.1016/j.cell.2016.04.038
1087 (2016).
1088
1089 Perotti, M. F., Ribone, P. A., Chan, R. L. Plant transcription factors from the
1090 Homeodomain-Leucine Zipper family I. Role in development and stress responses.
1091 *IUBMB Life* 69(5), 280-289. https://doi.org/10.1002/iub.1619 (2017).
1092
1093 Perotti M.F., Ribone P.A., Cabello J.V., Ariel F.D., Chan R.L. AtHB23 participates in the
1094 gene regulatory network controlling root branching, and reveals differences between
1095 secondary and tertiary roots. *Plant J.* 100(6), 1224-1236.
1096 https://doi.org/10.1111/tpj.14511 (2019).
1097
1098 Perotti, M. F., Ariel, F. D., Chan, R. L. Lateral root development differs between main
1099 and secondary roots and depends on the ecotype. *Plant Signal. Behav.* 15(6), 1755504.
1100 https://doi.org/10.1080/15592324.2020.1755504 (2020).
1101
1102 Perotti, M. F., Arce, A. L., Chan, R. L. The underground life of homeodomain-leucine
1103 zipper transcription factors. *J. Exp. Bot*. 72(11), 4005–4021.
1104 https://doi.org/10.1093/jxb/erab112 (2021).
1105
1106 Perotti, M. F., Arce, A. L., Ariel, F. D., Figueroa, C. M., Chan, R. L. The transcription factor
1107 AtHB23 modulates starch turnover for root development and plant survival under
1108 salinity. *Environ. Exp. Bot.* 201(11), 104994.
1109 https://doi.org/10.1016/j.envexpbot.2022.104994 (2022).
1110
1111 Perotti, M. F., Arce, A. L., Chan, R. L. The underground life of homeodomain-leucine
1112 zipper transcription factors. J. Exp. Bot. 72(11), 4005–4021.
1113 https://doi.org/10.1093/jxb/erab112 (2021).
1114
1115 Proust, H., Honkanen, S., Jones, V. A., Morieri, G., Prescott, H., Kelly, S., Ishizaki, K.,
1116 Kohchi, T., Dolan, L. *RSL* class I genes controlled the development of epidermal
1117 structures in the common ancestor of land plants. *Curr. Biol.* 26(1), 93–99.
1118 https://doi.org/10.1016/j.cub.2015.11.042 (2016).
1119
1120 Rasmussen, S., Barah, P., Suarez-Rodriguez, M. C., Bressendorff, S., Friis, P., Costantino,
1121 P., et al. (2013). Transcriptome responses to combinations of stresses in Arabidopsis.
1122 Plant Physiol. 161, 1783–1794. doi: 10.1104/pp.112.21077
1123
1124 Ribone, P., Capella, M., Chan, R. Functional characterization of the homeodomain
1125 leucine zipper I transcription factor AtHB13 reveals a crucial role in Arabidopsis

development. *J. Exp. Bot.* 66(19), 5929-5943. https://doi.org/10.1093/jxb/erv302 (2015).

Riechmann, J. L., Heard, J., Martin, G. ,Reuber L., Jiang C.,Keddie J., Adam L., Pineda O.,Ratcliffe O.J., Samaha R.R., Creelman R., Pilgrim M., Broun P., Zhang J. Z., Ghandehari D., Sherman B.K. , Yu G. Arabidopsis transcription factors: genome-wide comparative analysis among eukaryotes. *Science* 290(5499), 2105–2110. https://doi.org/10.1126/science.290.5499.2105 (2000).

Robinson, M. D., McCarthy, D. J., Smyth, G.K. edgeR: a Bioconductor package for differential expression analysis of digital gene expression data. *Bioinformatics* 26(1), 139-40. https://doi.org/10.1093/bioinformatics/btp616 (2010).

Rubio, V., Linhares, F., Solano, R., Martín, A. C., Iglesias, J., Leyva, A., Paz-Ares, J. A conserved MYB transcription factor involved in phosphate starvation signaling both in vascular plants and in unicellular algae. *Genes Dev*. 15(16), 2122–2133. https://doi.org/10.1101/gad.204401 (2001).

Ryu, K. H., Huang, L., Kang, H., Schiefelbein, J. Single-Cell RNA Sequencing Resolves Molecular Relationships Among Individual Plant Cells. *Plant Physiol*. 179(4), 1444-1456 https://doi.org/10.1104/pp.18.01482 (2019).

Silva, A. T., Ribone, P. A., Chan, R. L., Ligterink, W., Hilhorst, H. W. M. A predictive coexpression network identifies novel genes controlling the seed-to-seedling phase transition in Arabidopsis thaliana. *Plant Physiol*. 170(4), 2218–2231. https://doi.org/10.1104/pp.15.01704 (2016).

Silva-Navas, J., Moreno-Risueno, M. A., Manzano, C., Téllez-Robledo, B., Navarro-Neila, S., Carrasco, V., Pollmann, S., Gallego, F. J., del Pozo, J. C. Flavonols mediate root phototropism and growth through regulation of proliferation to-differentiation transition. *Plant Cell* 28(6), 1372–1387. https://doi.org/10.1105/tpc.15.00857 (2016).

Silva-Navas, J., Moreno-Risueno, M. A., Manzano, C., Pallero-Baena, M., Navarro-Neila, S., Téllez-Robledo, B., Garcia-Mina, J. M., Baigorri, R., Gallego, F. J., del Pozo, J. C. D-Root: a system for cultivating plants with the roots in darkness or under different light conditions. *Plant J.* 84(1), 244-255. https://doi.org/10.1111/tpj.12998 (2015).

Shibata, M., Breuer, C., Kawamura, A., Clark, N. M., Rymen, B., Braidwood, L., Morohashi, K., Busch, W., Benfey, P. N., Sozzani, R., Keiko, S. GTL1 and DF1 regulate root hair growth through transcriptional repression of ROOT HAIR DEFECTIVE 6-LIKE 4 in

1166 Arabidopsis. *Development* 145(3), dev159707. https://doi.org/10.1242/dev.159707
1167 (2018).
1168
1169 Shibata, M., Favero, D. S., Takebayashi, R., Takebayashi, A., Kawamura, A., Rymen, B.,
1170 Hosokawa, Y., Sugimoto, K. Trihelix transcription factors GTL1 and DF1 prevent aberrant
1171 root hair formation in an excess nutrient condition. *New Phytol.* 235(4), 1426-1441.
1172 https://doi.org/10.1111/nph.18255 (2022).
1173
1174 Shulse, C. N., Cole, B. J., Ciobanu, D., Lin, J., Dickel, D. E. High-throughput single-cell
1175 transcriptome profiling of plant cell types. *Cell Rep.* 27(7), 2241-2247.
1176 https://doi.org/10.1016/j.celrep.2019.04.054 (2019).
1177
1178 Spies, F. P., Raineri, J., Miguel, V. N., Cho, Y., Hong, J. C., Chan, R. L. The Arabidopsis
1179 transcription factors AtPHL1 and AtHB23 act together promoting carbohydrate
1180 transport from pedicel-silique nodes to seeds. *Plant Sci.* 315, 111133.
1181 https://doi.org/10.1016/j.plantsci.2021.111133 (2022).
1182
1183 Spies, F. P., Perotti, M. F., Cho, Y., Ig Jo, C., Hong J. C., Chan, R. L. A complex tissue-
1184 specific interplay between the Arabidopsis transcription factors AtMYB68, AtHB23, and
1185 AtPHL1 modulates primary and lateral root development and adaptation to salinity.
1186 *Plant J.* 115(4), 952-966. https://doi.org/10.1111/tpj.16273 (2023).
1187
1188 Vijayakumar, P., Datta, S. & Dolan, L. ROOT HAIR DEFECTIVE SIX-LIKE4 (RSL4) promotes
1189 root hair elongation by transcriptionally regulating the expression of genes required for
1190 cell growth. *New Phytol.* 212(4), 944-953. https://doi.org/10.1111/nph.14095 (2016).
1191
1192 Viola, I. L., Gonzalez, D. H., Chapter 6. Structure and evolution of plant homeobox genes,
1193 in: D.H. Gonzalez (Ed.), Plant Transcription Factors, Elsevier, 2016, pp. 101–112.
1194 https://doi.org/10.1016/B978-0-12-800854-6.00006-3 (2016).
1195
1196 Wu, J., Kurten, E. L., Monshausen, G., Hummel, G. M., Gilroy, S., Baldwin, I. T. NaRALF, a
1197 peptide signal essential for the regulation of root hair tip apoplastic pH in *Nicotiana*
1198 *attenuata*, is required for root hair development and plant growth in native soils. *Plant J.*
1199 52(5), 877-890. https://doi.org/10.1111/j.1365-313X.2007.03289.x (2007).
1200
1201 Yi, K., Menand, B., Bell, E., Dolan, L. A basic helix-loop-helix transcription factor controls
1202 cell growth and size in root hairs. *Nat. Genet. 42*(3), 264–267.
1203 https://doi.org/10.1038/ng.529 (2010).
1204

1205 Yu, G., Wang, L. G., Han, Y., He, Q. Y. ClusterProfiler: an R package for comparing
1206 biological themes among gene clusters. *OMICS*. 16(5), 284-287.
1207 https://doi.org/10.1089/omi.2011.0118 (2012).
1208
1209 Zhang, T., Xu, Z.,Shang, G.,Wang, J. A Single-Cell RNA Sequencing Profiles the
1210 Developmental Landscape of Arabidopsis Root. *Mol. Plant* 12(5), 648-660.
1211 https://doi.org/10.1016/j.molp.2019.04.004 (2019).
1212
1213 Zhu, S., Estevez, J. M., Liao, H., Zhu, Y., Yang, T., Li, C., Wang, Y., Li, L., Liu, X., Martinez-
1214 Pacheco, J., Guo, H., Yu, F. The RALF1–FERONIA Complex Phosphorylates eIF4E1 to
1215 Promote Protein Synthesis and Polar Root Hair Growth. *Mol. Plant* 13(5), 698-716.
1216 https://doi.org/10.1016/j.molp.2019.12.014 (2020a).
1217
1218 Zhu, S., Martínez-Pacheco, J., Estevez, J. M. & Yu, F. Autocrine regulation of root hair
1219 size by the RALF-FERONIA-RSL4 signaling pathway. *New Phytol*. 227(1), 45-49.
1220 https://doi.org/10.1111/nph.16497 (2020b).